

Second order semi-parametric inference for multivariate log Gaussian Cox processes

Kristian Bjørn Hesselund¹, Ganggang Xu², Yongtao Guan² and Rasmus Waagepetersen¹

¹Department of Mathematical Sciences, Aalborg University

²Department of Management Science, University of Miami

July 2, 2022

Abstract

This paper introduces a new approach to inferring the second order properties of a multivariate log Gaussian Cox process (LGCP) with a complex intensity function. We assume a semi-parametric model for the multivariate intensity function containing an unspecified complex factor common to all types of points. Given this model we exploit the availability of several types of points to construct a second-order conditional composite likelihood to infer the pair correlation and cross pair correlation functions of the LGCP. Crucially this likelihood does not depend on the unspecified part of the intensity function. We also introduce a cross validation method for model selection and an algorithm for regularized inference that can be used to obtain sparse models for cross pair correlation functions. The methodology is applied to simulated data as well as data examples from microscopy and criminology. This shows how the new approach outperforms existing alternatives where the intensity functions are estimated non-parametrically.

Keywords: case-control, composite likelihood, conditional likelihood, cross pair correlation function, multivariate, pair correlation function, point process.

1 Introduction

A multivariate or multi-type point pattern is a marked point pattern where the marks belong to a finite set corresponding to different types of points. Equivalently, a multivariate point pattern can be viewed as a finite collection of ordinary point patterns, where each of these point patterns consists of points of a specific type. In this paper we consider point pattern data from biology and criminology. In the former case the point pattern represents locations of different types of cells in a tumor and in the latter case crime scenes of different types of crimes. An obvious key point of interest is then to study possible associations between the points of different types.

If consistent estimates of the intensity functions are available, and under assumptions of second-order intensity reweighted stationarity (Baddeley et al., 2000) or intensity-reweighted moment stationarity (van Lieshout, 2011), an immediate approach is to compute non-parametric cross summary statistics such as cross K , cross pair correlation, or cross J functions (Møller and Waagepetersen, 2003; Baddeley et al., 2014; Cronie and van Lieshout, 2016). Parametric estimation of cross associations is also possible, see e.g. Jalilian et al. (2015); Waagepetersen et al. (2016); Choiruddin et al. (2019) who used parametric models of intensity and pair correlation functions, or Rajala et al. (2018) who specified a full model in terms of a multivariate Markov point process.

In some cases it is not straightforward to estimate the intensity function. For the cells data considered in this paper, the intensities of each type appear to be very heterogeneous, possibly varying within regions corresponding to different types of tissue. However, it is not straightforward to delineate these regions. For the crime data considered, the intensity functions depend in a complex manner on the urban structures and the population density.

In case of bivariate case-control processes, Diggle et al. (2007) suggested a semi-parametric model where complex features of the case and control intensity functions were captured by a common non-parametric factor. This factor was estimated non-parametrically from the control point process and next used in a semi-parametric estimate of the intensity function for the case process. Finally this estimate was plugged into an estimate of the K -function for the case process. Using the control process to estimate the non-parametric part of the case intensity function mitigates the problem of confounding of possible clustering in the case process with variations in the case intensity function. However, sensitivity to the choice of bandwidth for the non-parametric estimation remains. Also the case and control processes were assumed to be independent whereby the cross pair correlation function is restricted to be one. Diggle et al. (2007) assumed the control process to be Poisson and Henrys and Brown (2009) relaxed this assumption by allowing both case and control processes to be clustered. They however retained independence between the two processes. Guan et al. (2008) used the same framework as Diggle et al. (2007) but used a second-order conditional composite likelihood to fit a parametric model to the case pair correlation function. The composite likelihood notably did not depend on the non-parametric part of the case intensity function and hence avoided choosing a bandwidth for non-parametric estimation.

In the context of multivariate point processes, Hesselund et al. (2019) used a semi-parametric model for the multivariate intensity function assuming a multiplicative structure where for each type of points, the intensity function is a product of a common background intensity and a log-linear factor modeling effects of covariates. Hence focus is on estimating differences between the intensity functions (for different types of points) that can be explained in terms of the covariates. In the bivariate case this model coincides with the one used in Diggle et al. (2007). However, Hesselund et al. (2019) did not impose any restrictive assumptions regarding the correlations within each type of points or between different types of points. While the main focus in Hesselund et al. (2019) was inference for the intensity function, they also obtained non-parametric estimates of ratios of cross pair correlation func-

tions. They were, however, not able to obtain estimates of the individual cross pair correlation functions.

Our objective in this paper is to infer the full within and between correlation structure of a multivariate point process. To do so we adopt the parametric log Gaussian Cox process (LGCP) model for the correlation structure proposed in Waagepetersen et al. (2016) and further considered in Choiruddin et al. (2019). This model is flexible and has a very natural interpretation in terms of latent structures. However, to deal with complex intensity functions, we replace the parametric model for the intensity function used in Waagepetersen et al. (2016) with the semi-parametric model for the intensity function from Hesselund et al. (2019). In this way we combine the strengths of two modelling approaches.

The presence of a non-parametric factor in the intensity function means that ingenuity is needed for fitting the parametric part of the model. We generalize the approach for the bivariate case in Guan et al. (2008) and obtain a second order conditional composite likelihood function which only depends on the parametric parts of the model and hence does not require knowledge of the non-parametric component. Compared with Guan et al. (2008) we consider an arbitrary number of point processes and do not assume that any of the point processes are Poisson nor that any two point processes are uncorrelated.

Some key questions we want to address for a particular data set are whether some point processes are uncorrelated and if not, whether they are negatively or positively correlated. We address these questions by a model selection approach where the models considered represent different types of correlation structures. Absence of correlation between point processes requires that certain parameters must be zero. To enable selection of models with parameters set to zero we combine our semi-parametric composite likelihood with a Lasso penalization (Tibshirani, 1996) which precisely facilitates that some parameters can be estimated to be exactly zero. A similar approach was considered by Choiruddin et al. (2019) in the context of least squares estimation for a multivariate LGCP with a full parametric model for the multivariate intensity function.

The rest of the paper is organized as follows. Section 2 gives a brief overview of multivariate point processes with focus on the intensity functions and cross intensity functions. Next the semi-parametric model for the intensity function and the multivariate LGCP model is described. Section 3 introduces the second order conditional composite likelihood function, an optimization algorithm based on the proximal Newton method, and a cross validation method for model selection. Section 4 contains simulation studies and Section 5 applies our methodology to cells and crimes data sets. Some concluding remarks are given in Section 6.

2 Semi-parametric modelling of a multivariate point process

2.1 Background on intensity functions

Let $\mathbf{X} = (X_1, \dots, X_p)$ be a multivariate spatial point process, where X_i is a spatial point process on \mathbb{R}^d representing points of type i , $i = 1, \dots, p$. Each X_i is hence a random subset of \mathbb{R}^d such that the cardinality of $X_i \cap B$ is finite almost surely for any bounded $B \subset \mathbb{R}^d$. In practice we observe \mathbf{X} in a spatial window W , where the window $W \subset \mathbb{R}^d$ is bounded with area $|W| > 0$. We will assume there exist for each $i, j = 1, \dots, p$, non-negative functions $\rho_i(\cdot)$ and $\rho_{ij}(\cdot)$ so that the so-called Campbell's formulae:

$$\mathbb{E} \sum_{\mathbf{u} \in X_i} h_1(\mathbf{u}) = \int h_1(\mathbf{u}) \rho_i(\mathbf{u}) d\mathbf{u} \quad (1)$$

$$\mathbb{E} \sum_{\substack{\neq \\ \mathbf{u} \in X_i, \mathbf{v} \in X_j}} h_2(\mathbf{u}, \mathbf{v}) = \int h_2(\mathbf{u}, \mathbf{v}) \rho_{ij}(\mathbf{u}, \mathbf{v}) d\mathbf{u} d\mathbf{v}, \quad (2)$$

hold for any non-negative functions $h_1(\cdot)$ and $h_2(\cdot, \cdot)$, where \sum^{\neq} means that the sum is over pairwise distinct pairs (\mathbf{u}, \mathbf{v}) . The function $\rho_i(\cdot)$ is called the intensity function of X_i . If $i = j$, then $\rho_{ii}(\cdot)$ is called the second order intensity function of X_i , while if $i \neq j$, $\rho_{ij}(\cdot)$ is called the cross intensity function between X_i and X_j . The normalized cross intensity function, called cross pair correlation function (cross PCF), is denoted by $g_{ij}(\cdot)$ and defined by: $\rho_i(\mathbf{u}) \rho_j(\mathbf{v}) g_{ij}(\mathbf{u}, \mathbf{v}) = \rho_{ij}(\mathbf{u}, \mathbf{v})$. If $i = j$ we just call $g_{ii}(\cdot)$ the pair correlation function (PCF) for X_i . If X_i and X_j are independent, then $g_{ij}(\mathbf{u}, \mathbf{v}) = 1$ while $g_{ij}(\mathbf{u}, \mathbf{v}) > 1$ (< 1) is indicative of positive (negative) association between X_i and X_j (or between points in X_i in the case $i = j$). Hence the cross PCFs provide useful insight regarding the dependence within and between the point processes. We assume that X is second order cross intensity reweighted stationary and isotropic, i.e., with an abuse of notation, $g_{ij}(\mathbf{u}, \mathbf{v}) = g_{ij}(r)$, $i, j = 1, \dots, p$, where $r = \|\mathbf{u} - \mathbf{v}\|$.

2.2 Semi-parametric regression model for the intensity

It may sometimes be difficult to specify a simple parametric model for the intensity functions. One may then resort to non-parametric estimation of the intensity functions but the results depend heavily on the choice of smoothing bandwidth where different data driven methods may result in very different results, see e.g. simulation studies in Cronie and van Lieshout (2018) and Shaw et al. (2020). We instead consider a semi-parametric model where a background intensity function $\rho_0(\cdot)$ captures complex variation in the intensity function that is common to all the point processes X_1, \dots, X_p . For the cells data considered in Section 5.1, $\rho_0(\cdot)$ may capture variations in tissue composition that influence occurrence of different types of cells while for the crime data in Section 5.2, $\rho_0(\cdot)$ captures variation in population density and dependence of the intensities on the urban structure. More specifically, following

Hessellund et al. (2019), we consider the multiplicative model:

$$\rho_i(\mathbf{u}; \boldsymbol{\gamma}_i) = \rho_0(\mathbf{u}) \exp(\boldsymbol{\gamma}_i^\top \mathbf{z}(\mathbf{u})) \quad (3)$$

for the intensity of X_i where $\mathbf{z}(\mathbf{u})$ denotes a vector of spatial covariates at location \mathbf{u} and $\boldsymbol{\gamma}_i$ is a regression parameter vector.

Since $\rho_0(\cdot)$ is left completely unspecified, the parameters $\boldsymbol{\gamma}_i$ are not identifiable: replacing the l th entry γ_{il} in $\boldsymbol{\gamma}_i$ by $\gamma_{il} - K$ for $i = 1, \dots, p$ while replacing $\rho_0(\cdot)$ by $\rho_0(\cdot) \exp(K \mathbf{z}_l(\mathbf{u}))$ does not change the model when $\rho_0(\cdot)$ is unspecified. Hessellund et al. (2019) proposed methodology for estimating contrasts $\boldsymbol{\beta}_i = \boldsymbol{\gamma}_i - \boldsymbol{\gamma}_p$ where $\boldsymbol{\beta}_p = 0$. Alternatively, one could impose sum-to-zero constraints $\sum_l \boldsymbol{\beta}_{il} = 0$ on the $\boldsymbol{\beta}_i$.

Given the semi-parametric model for the intensity functions and its associated estimation procedure we specify in the next section a model for the correlation structure of the multivariate point process.

2.3 Multivariate log Gaussian Cox model

Following the setup in Waagepetersen et al. (2016), we assume that X_i for $i = 1, \dots, p$, is a Cox process with random intensity given by:

$$\Lambda_i(\mathbf{u}) = \rho_0(\mathbf{u}) \exp(\boldsymbol{\gamma}_i^\top \mathbf{z}(\mathbf{u})) \exp \left(\mu_i + \sum_{k=1}^q \alpha_{ik} Y_k(\mathbf{u}) + \sigma_i U_i(\mathbf{u}) \right), \quad (4)$$

where the Y_k and U_i are independent zero mean unit variance Gaussian random fields and $\mu_i = -\sum_{k=1}^q \alpha_{ik}^2/2 - \sigma_i^2/2$. We interpret the Y_k as latent random factors that influence all types of points. Hence the different types of points may be correlated due to possible dependence on the Y_k . Moreover, each U_i is a type-specific random factor that only affects the i th type of points. Hence U_i models random clustering within each X_i .

Consider for a moment the ideal situation where the Y_k are observed (non-random). Following the same considerations as for the $\boldsymbol{\gamma}_i$ in the previous section we should then impose restrictions $\alpha_{pl} = 0$ or $\sum_{i=1}^p \alpha_{il} = 0$, $l = 1, \dots, q$, in order to ensure identifiability. In case of unobserved Y_k and hence less information, the need for a constraint is not less pertinent. In the following we impose the sum-to-zero constraint $\sum_{i=1}^p \alpha_{il} = 0$, $l = 1, \dots, q$ which treats all X_i symmetrically.

The intensity function of X_i is $\rho_i(\mathbf{u}) = \mathbb{E}[\Lambda_i(\mathbf{u})] = \rho_0(\mathbf{u}) \exp(\boldsymbol{\gamma}_i^\top \mathbf{z}(\mathbf{u}))$, which follows from the moment generating function of a Gaussian random variable. Similarly,

$$\begin{aligned} \rho_{ij}(\mathbf{u}, \mathbf{v}) &= \mathbb{E}[\Lambda_i(\mathbf{u}) \Lambda_j(\mathbf{v})] = \rho_0(\mathbf{u}) \rho_0(\mathbf{v}) \exp(\boldsymbol{\gamma}_i^\top \mathbf{z}(\mathbf{u})) \exp(\boldsymbol{\gamma}_j^\top \mathbf{z}(\mathbf{v})) \\ &\quad \times \exp \left(\sum_{k=1}^q \alpha_{ik} \alpha_{jk} c_{Y_k}(\mathbf{u}, \mathbf{v}) + 1[i=j] \sigma_i^2 c_{U_i}(\mathbf{u}, \mathbf{v}) \right), \end{aligned}$$

where $c_{Y_k}(\mathbf{u}, \mathbf{v}) = \text{Corr}[Y_k(\mathbf{u}), Y_k(\mathbf{v})]$ and $c_{U_i}(\mathbf{u}, \mathbf{v}) = \text{Corr}[U_i(\mathbf{u}), U_i(\mathbf{v})]$.

For $c_{Y_k}(\cdot)$ and $c_{U_i}(\cdot)$ we use exponential correlation functions, i.e. $c_{Y_k}(\mathbf{u}, \mathbf{v}) = \exp(-\|\mathbf{u} - \mathbf{v}\|/\xi_k)$ and $c_{U_i}(\mathbf{u}, \mathbf{v}) = \exp(-\|\mathbf{u} - \mathbf{v}\|/\phi_i)$ with correlation scale parameters ξ_k and ϕ_i . Other parametric correlation models might of course be used

instead, depending on the application. Denote by $\boldsymbol{\theta}$ the concatenation of $\boldsymbol{\alpha}_k = (\alpha_{1k}, \dots, \alpha_{pk})^\top$, $k = 1, \dots, q$, $\boldsymbol{\xi} = (\xi_1, \dots, \xi_q)^\top$, $\boldsymbol{\sigma}^2 = (\sigma_1^2, \dots, \sigma_p^2)^\top$, and $\boldsymbol{\phi} = (\phi_1, \dots, \phi_p)^\top$. The cross PCF between X_i and X_j is then given by the parametric model:

$$g_{ij}(r; \boldsymbol{\theta}) = \exp\left(\sum_{k=1}^q \alpha_{ik}\alpha_{jk}\exp(-r/\xi_k) + 1[i=j]\sigma_i^2\exp(-r/\phi_i)\right). \quad (5)$$

If $\sum_{k=1}^q \alpha_{ik}\alpha_{jk}\exp(-r/\xi_k)$ is greater (smaller) than 0, this implies positive (negative) spatial correlation between points from X_i and X_j at the lag r . If for example $\alpha_{ik}\alpha_{jk} = 0$ for all $k = 1, \dots, q$, then X_i and X_j are independent.

The number q of latent common fields controls the complexity of the model and will be chosen according to a cross validation criterion detailed in Section 3.3. In Waagepetersen et al. (2016) and Choiruddin et al. (2019), estimation of $\boldsymbol{\theta}$ for a chosen q was based on a least squares criterion where non-parametric estimates of the pair correlation function acted as ‘dependent’ variables. These non-parametric estimates were based on fully specified regression models for the log intensity functions that are not available in our current setting. Section 3 therefore introduces a second order conditional composite likelihood function for estimation of $\boldsymbol{\theta}$ that does not require knowledge of $\rho_0(\cdot)$.

3 Second order conditional composite likelihood

We assume initially that the β_i are known and thus suppress dependence on these in the notation. The idea is to condition on the union of all points regardless of type and for each $\mathbf{u} \neq \mathbf{v} \in \cup_{i=1}^p X_i$ consider the conditional probability (see Section A) that \mathbf{u} is of type i and \mathbf{v} is of type j :

$$p_{ij}(\mathbf{u}, \mathbf{v}; \boldsymbol{\theta}) = \frac{\rho_{ij}(\mathbf{u}, \mathbf{v})}{\sum_{k,l} \rho_{kl}(\mathbf{u}, \mathbf{v})} = \frac{f_i(\mathbf{u})f_j(\mathbf{v})g_{ij}(r; \boldsymbol{\theta}_{ij})}{\sum_{k,l} f_k(\mathbf{u})f_l(\mathbf{v})g_{kl}(r; \boldsymbol{\theta}_{kl})}, \quad (6)$$

where $f_i(\mathbf{u}) = \exp(\beta_i^\top \mathbf{z}(\mathbf{u}))$, $i = 1, \dots, p$. Note that $\rho_0(\mathbf{u})\rho_0(\mathbf{v})$ cancels out in (6) so that the probabilities do not depend on the unspecified $\rho_0(\cdot)$. We then estimate $\boldsymbol{\theta}$ by maximizing the second order conditional composite likelihood function given by:

$$L(\boldsymbol{\theta}) = \prod_{i,j} \prod_{\substack{\mathbf{u} \in X_i \cap W, \mathbf{v} \in X_j \cap W \\ \mathbf{u} \neq \mathbf{v}}} 1_R[\mathbf{u}, \mathbf{v}] p_{ij}(\mathbf{u}, \mathbf{v}; \boldsymbol{\theta}), \quad (7)$$

where $1_R[\mathbf{u}, \mathbf{v}] = 1[||\mathbf{u} - \mathbf{v}|| \leq R]$ and $R > 0$ is a user-specified tuning parameter. Specifying an $R < \infty$ is useful for reducing computing time and can also improve the statistical efficiency by omitting pairs of points \mathbf{u} and \mathbf{v} that are distant from each other and hence do not provide much information on the correlation structure. As a rule of thumb, R should be chosen so that $g_{ij}(r; \boldsymbol{\theta}) \approx 1$ for $||\mathbf{u} - \mathbf{v}|| > R$. Methods for choosing R are discussed in Lavancier et al. (2019).

The cross PCFs (5) and hence the second order conditional composite likelihood function are invariant to simultaneous interchange of columns $\boldsymbol{\alpha}_k = (\alpha_{ik})_k$ and

corresponding correlation scale parameters ξ_k as well as to multiplication by -1 of α_k . This lack of identifiability is not of much concern since we are not interested in the individual α_{ij} 's but rather the resulting correlation structure which is invariant to the aforementioned transformations.

Following the idea of two-step estimation in Waagepetersen and Guan (2009), we replace the parameters β_i by consistent estimates $\hat{\beta}_i$ obtained using the method proposed in Hessellund et al. (2019) that does not require knowledge of θ .

3.1 Optimization

We denote by $l_-(\theta)$ the negation of the log of (7) and turn the estimation of θ into a minimization problem. In order to minimize $l_-(\theta)$ with respect to θ , we consider a cyclic block descent algorithm. The strategy is to update α , ξ , σ^2 and ϕ in turn until a convergence criterion is met. In the following we will, with a convenient abuse of notation, use α to denote both the matrix $[\alpha_{ij}]_{ij}$ and the vectorized version where the matrix is laid out column-wise $(\alpha_1^\top, \dots, \alpha_q^\top)^\top$. It will be clear from the context which interpretation of α is relevant. Denote by $\theta^{(n)} = ((\alpha^{(n)})^\top, (\xi^{(n)})^\top, (\sigma^{2(n)})^\top, (\phi^{(n)})^\top)^\top$ the current value of θ . We update each parameter using a quasi Newton-Raphson iteration with additional line search. This is equivalent to minimizing a certain least squares problem. We give the details of this since this is also needed for solving a regularized version of our estimation problem, see Section 3.2.

We denote by $\tilde{\theta}$ a temporary parameter vector that keeps track of the updates leading from $\theta^{(n)}$ to $\theta^{(n+1)}$ and initialize $\tilde{\theta} = \theta^{(n)}$. Denote by $\tilde{\tau} \in \{\tilde{\alpha}, \tilde{\xi}, \tilde{\sigma}^2, \tilde{\phi}\}$ the parameter vector to be updated and by $\tilde{\theta}(\tau)$ the vector obtained by replacing $\tilde{\tau}$ in $\tilde{\theta}$ by τ . Consider a quadratic approximation of $l_-(\tilde{\theta}(\tau))$ with respect to τ around $\tilde{\theta}$:

$$q(\tau) = l_-(\tilde{\theta}) + (\tau - \tilde{\tau})^\top \text{e}(\tilde{\tau}) + \frac{1}{2}(\tau - \tilde{\tau})^\top \text{H}(\tilde{\tau})(\tau - \tilde{\tau}). \quad (8)$$

Here (omitting for convenience the arguments \mathbf{u}, \mathbf{v})

$$\text{e}(\tau) = \nabla_\tau l_-(\tilde{\theta}(\tau)) = \sum_{i,j} \sum_{\substack{\mathbf{u} \in X_i \cap W \\ \mathbf{v} \in X_j \cap W}}^{\neq} 1_R \left(\frac{\sum_{k,l} \nabla_\tau \rho_{kl}(\tilde{\theta}(\tau))}{\sum_{k,l} \rho_{kl}(\tilde{\theta}(\tau))} - \frac{\nabla_\tau \rho_{ij}(\tilde{\theta}(\tau))}{\rho_{ij}(\tilde{\theta}(\tau))} \right)$$

is the gradient with respect to τ and

$$\text{H}(\tau) = \text{E}[\nabla_\tau^2 l_-(\tilde{\theta}(\tau))] = \int_{W^2} 1_R \text{Cov} \left(Z(\tilde{\theta}(\tau)) \right) \sum_{i,j} \rho_{ij}(\tilde{\theta}(\tau)) d\mathbf{u} d\mathbf{v}$$

is the expected Hessian with respect to τ , where $Z(\mathbf{u}, \mathbf{v}, \tilde{\theta}(\tau))$ denotes a random vector which takes values $\nabla_\tau \log(\rho_{ij}(\mathbf{u}, \mathbf{v}; \tilde{\theta}(\tau)))$ with probabilities $p_{ij}(\mathbf{u}, \mathbf{v}; \tilde{\theta}(\tau))$ (Lemma B.2). We estimate $\text{H}(\tilde{\tau})$ by

$$\hat{\text{H}}(\tilde{\tau}) = \sum_{i,j} \sum_{\substack{\mathbf{u} \in X_i \cap W, \mathbf{v} \in X_j \cap W}}^{\neq} 1_R[\mathbf{u}, \mathbf{v}] \text{Cov} \left(Z(\mathbf{u}, \mathbf{v}, \tilde{\theta}) \right),$$

which is unbiased by (2). Since $\hat{H}(\tilde{\tau})$ is a symmetric, positive semi-definite matrix, the eigendecomposition implies that $\hat{H}(\tilde{\tau})^{1/2} = UD^{1/2}U^\top$, where D is the diagonal matrix of the (all non-negative) eigen values of $\hat{H}(\tilde{\tau})$ and U is the matrix with the eigen vectors as columns. Assuming that all the eigen values are positive, following Section C, the minimizer $\hat{\tau}$ of (8) is a solution of a least squares problem:

$$\hat{\tau} = \arg \min_{\tau} \left(\frac{1}{2} \|Y - X\tau\|^2 \right) = (X^\top X)^{-1} X^\top Y, \quad (9)$$

where $Y = \hat{H}(\tilde{\tau})^{1/2} \left(-\hat{H}(\tilde{\tau})^{-1} e(\tilde{\tau}) + \tilde{\tau} \right)$ and $X = \hat{H}(\tilde{\tau})^{1/2}$. Introducing a line search, we update $\tau^{(n+1)} = \tilde{\tau} + t(\hat{\tau} - \tilde{\tau})$, for some $t > 0$ and also update $\tilde{\theta}$ by replacing $\tilde{\tau} = \tau^{(n)}$ by $\tau^{(n+1)}$. When all components of $\tilde{\theta}$ have been updated we let $\theta^{(n+1)} = \tilde{\theta}$.

As mentioned in Section 2.3 we impose a sum to zero constraint on each α_k , i.e. $\sum_{i=1}^p \alpha_{ik} = 0$, $k = 1, \dots, q$. The constraint is easily accommodated by the change of variable $B\psi = \alpha$, where ψ is a $(p-1) \times q$ matrix and $B^\top = [I_{p-1} \ -\mathbf{1}]$ is a $(p-1) \times p$ matrix, where I_{p-1} is the $(p-1) \times (p-1)$ identity matrix and $-\mathbf{1} = [-1, \dots, -1]^\top \in \mathbb{R}^p$. Under the sum to zero constraint, the relation between α and ψ is one-to-one. Thus in case of $\tau = \alpha$ we update the unconstrained parameter ψ using, by the chain rule, the gradient $B^\top e(\tilde{\theta})$ and the Hessian $B^\top H(\tilde{\theta}) B$ and finally let $\alpha^{(n+1)} = B\psi^{(n+1)}$.

The cyclical block updating is iterated until relative function convergence,

$$\left| \left[l_- \left(\theta^{(n+1)} \right) - l_- \left(\theta^{(n)} \right) \right] / l_- \left(\theta^{(n)} \right) \right| < \epsilon, \quad (10)$$

for some $\epsilon > 0$ in which case we set $\hat{\theta} = \theta^{(n+1)}$. Algorithm 1 gives a brief overview of the cyclical block descent algorithm.

Algorithm 1 Cyclical block descent algorithm

- 1: Simulate initial parameters $\hat{\psi}^{(0)}$, $\hat{\xi}^{(0)}$, $\hat{\sigma}^{2(0)}$ and $\hat{\phi}^{(0)}$
 - 2: $n := 0$
 - 3: **repeat**
 - 4: $\tilde{\psi} := \psi^{(n)}$, $\tilde{\xi} := \xi^{(n)}$, $\tilde{\sigma}^2 := \sigma^{2(n)}$ and $\tilde{\phi} := \phi^{(n)}$
 - 5: update $\tilde{\psi}$, $\tilde{\xi}$, $\tilde{\sigma}^2$ and $\tilde{\phi}$ in turn using (9) combined with line search
 - 6: $\psi^{(n+1)} := \tilde{\psi}$, $\xi^{(n+1)} := \tilde{\xi}$, $\sigma^{2(n+1)} := \tilde{\sigma}^2$, $\phi^{(n+1)} := \tilde{\phi}$, and $\alpha^{(n+1)} := B\psi^{(n+1)}$
 - 7: $n := n + 1$
 - 8: **until** relative convergence criterion (10)
 - 9: **return** $\hat{\theta} = \theta^{(n)}$
-

3.2 Optimization with lasso regularization

The overall model complexity is controlled by the number q of latent fields. Nevertheless, for any q , more sparse submodels could be obtained by restricting some α_{ij} , $i = 1, \dots, p$, $j = 1, \dots, q$ to zero. Of course if all entries in a column α_k are restricted to zero this just corresponds to reducing q by one. In order to look for sparse submodels for a given q we extend the estimation approach by introducing a

lasso regularization on α . We express the sum to zero constraint for α by $C\alpha = \mathbf{0}$, where $C = [D_1 \cdots D_q]$ is a $q \times pq$ matrix that consists of submatrices D_i , $i = 1, \dots, q$, of dimension $q \times p$. Each submatrix D_i consists of ones on the i th row and zeros otherwise. Here α should be interpreted as the vector obtained by concatenating the α_k , cf. Section 3.1. Note that the regularization is not relevant in the bivariate case $p = 2$ since in this case, by the sum to zero constraint, $\alpha_{1k} = 0$ implies $\alpha_{2k} = 0$ which just corresponds to reducing q by 1.

The regularized object function becomes:

$$l_-(\theta) + \lambda \sum_{i=1}^p \sum_{j=1}^q |\alpha_{ij}|, \quad C\alpha = \mathbf{0}, \quad (11)$$

where $\lambda \sum_{i=1}^p \sum_{j=1}^q |\alpha_{ij}|$ is a lasso penalty that can lead to exact zero components in the estimate of α . We minimize this using a cyclical block descent algorithm which only differs from the one in Section 3.1 by the update $\hat{\alpha} = \arg \min_{\alpha} \left(\frac{1}{2} \|Y - X\alpha\|^2 + \lambda \sum_{i=1}^p \sum_{j=1}^q |\alpha_{ij}| \right)$ subject to $C\alpha = \mathbf{0}$. To compute $\hat{\alpha}$ under the sum to zero constraint, we use the augmented Lagrangian algorithm suggested in Shi et al. (2016). Details are given in Section D. In Section 3.3 we propose a cross validation procedure to choose λ .

3.3 Determination of q and λ

We choose the values of q and λ according to a K -fold ($K \geq 2$) cross validation criterion constructed so that it targets selection of an appropriate cross correlation structure. Let for each i, j , M_{ij} denote the set of pairs (\mathbf{u}, \mathbf{v}) with $\mathbf{u} \in X_i$, $\mathbf{v} \in X_j$, and $0 < \|\mathbf{u} - \mathbf{v}\| \leq R$. We randomly split M_{ij} into K equally sized subsets $M_{ij,1}, \dots, M_{ij,K}$. We then obtain for each $k = 1, \dots, K$, a parameter estimate $\hat{\theta}_k$ by maximizing the regularized conditional composite likelihood

$$l_k(\theta) = \sum_{i,j} \sum_{(\mathbf{u}, \mathbf{v}) \in M_{ij,-k}}^{\neq} \log p_{ij}(\mathbf{u}, \mathbf{v}; \theta) + \lambda \sum_{i=1}^p \sum_{j=1}^q |\alpha_{ij}|, \quad C\alpha = \mathbf{0},$$

for the training data set consisting of the leave one fold out sets $M_{ij,-k} = \cup_{l \neq k} M_{ij,l}$. The k th cross validation score based on the validation sets $M_{ij,k}$, $i \neq j$, is then

$$CV_k(q, \lambda) = \sum_{i \neq j} \sum_{(\mathbf{u}, \mathbf{v}) \in M_{ij,k}} \log p_{ij}(\mathbf{u}, \mathbf{v}; \hat{\theta}_k).$$

We here omit the $M_{ii,k}$ to focus the cross validation on the fit of the cross correlation structure. To reduce the sensitivity to Monte Carlo variation, one may compute cross validation scores $CV_{kl}(q, \lambda)$, $l = 1, \dots, L$, based on L independent K -fold random splits of the data and use the average $\overline{CV}(q, \lambda)$ of the $CV_{kl}(q, \lambda)$, $k = 1, \dots, K$, $l = 1, \dots, L$. According to standard practice in the statistical learning literature (Hastie et al., 2013) we use K in the range of 5 to 10.

Consider the case $\lambda = 0$ which is relevant for example when $p = 2$. The most obvious choice of q is the one that minimizes the cross validation score,

$q_{\min} = \arg \min_q \overline{CV}(q, 0)$. We denote this the minimum (MIN) rule. However, due to sensitivity to Monte Carlo error, a so-called one standard error rule has been proposed (Hastie et al., 2013) that promotes more sparse solutions. Let $SD(q, 0)$ denote the standard deviation of a cross validation score $CV_{kl}(q, 0)$ obtained from a single validation set. In the current framework, the one standard error (1-SE) rule selects the smallest q (q_{1-SE}) for which $\overline{CV}(q, 0) \leq \overline{CV}(q_{\min}, 0) + SE(q_{\min}, 0)$, where $SE(q, 0) = SD(q_{\min}, 0)/\sqrt{KL}$ is the standard error of $\overline{CV}(q_{\min}, 0)$.

For joint selection of (q, λ) the immediate choice would be the minimizer of $\overline{CV}(q, \lambda)$. However, computing $\overline{CV}(q, \lambda)$ over a two-dimensional grid of q and λ values is very time consuming. Instead we use a two-step approach where we first determine q_{\min} as in the previous paragraph and next choose the λ that minimizes $\overline{CV}(q_{\min}, \lambda)$ over values of λ . Thus the initial selection of q determines the overall model complexity while the subsequent possible selection of a $\lambda > 0$ may introduce additional sparsity given q_{\min} .

3.4 Model assessment

Assuming the model (3) for the intensity functions, Hesselund et al. (2019) obtained a consistent non-parametric estimate of any ratio $g_{ij}(r)/g_{lk}(r)$ of cross PCFs, $r > 0$, $i, j, l, k = 1, \dots, p$. Similarly we can obtain semi-parametric estimates of these ratios based on our semi-parametric estimates of the cross PCFs. If the assumed multivariate LGCP is valid, the non-parametric and the semi-parametric estimates of cross PCF ratios should not differ much. In our data examples in Section 5 we informally assess the models by visual comparison of the two types of estimates. We also conduct a so-called global envelope goodness-of-fit test (Myllymäki et al., 2016) based on the difference between the two types of estimates over spatial lags $r \in [0, R]$. This requires simulation under a null model. For this we use the fitted multivariate LGCP where we replace the unknown background intensity ρ_0 by a non-parametric estimate introduced in Hesselund et al. (2019), see also Section E.

4 Simulation study

To study the performance of the package consisting of the second order conditional composite likelihood, the optimization algorithm in Section 3.1 with additional lasso regularization in Section 3.2, and the cross validation procedure, we conduct simulation studies based on two different settings for a five-variate LGCP $\mathbf{X} = (X_1, X_2, X_3, X_4, X_5)^\top$ on $W = [0, 1]^2$. In both cases we simulate one covariate $Z(\cdot)$ and a background intensity $\rho_0(\cdot) = 400 \exp(0.5V(\cdot) - 0.5^2/2)$, where Z and V are zero mean unit variance Gaussian random fields with exponential and Gaussian correlation functions, i.e. $\text{Corr}(Z(\mathbf{u}), Z(\mathbf{v})) = \exp(-\|\mathbf{u} - \mathbf{v}\|/0.05)$ and $\text{Corr}(V(\mathbf{u}), V(\mathbf{v})) = \exp(-(\|\mathbf{u} - \mathbf{v}\|/0.2)^2)$. The realizations of Z and ρ_0 are shown in Figure 1.

Table 1 shows the values used for all parameters except $\boldsymbol{\alpha}$ and $\boldsymbol{\xi}$ as well as the expected number of points N for each point process. Regarding q , $\boldsymbol{\alpha}$ and $\boldsymbol{\xi}$ we take $q = 0$ for the first setting resulting in a case with independent components X_1, \dots, X_5 . In the second setting we let $q = 2$ and choose $\boldsymbol{\alpha}$ as specified in the table

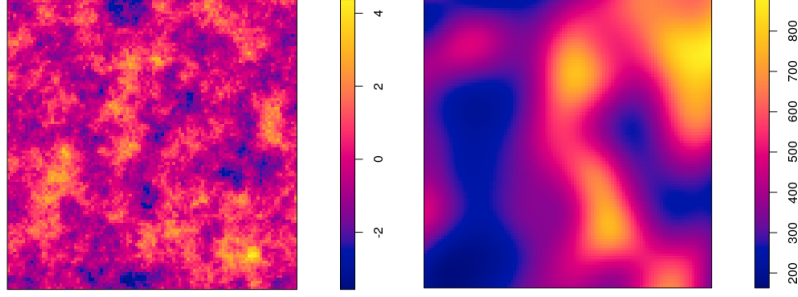


Figure 1: Left: simulated covariate Z . Right: simulated ρ_0 .

Table 1: Simulation settings for \mathbf{X} in each setup $q = 0, 2$ (excluding α and ξ).

\mathbf{X}	γ_1	γ_2	σ	ϕ	N	\mathbf{X}	γ_1	γ_2	σ	ϕ	N
X_1	0.1	-0.1	0.71	0.02	550	X_4	0.4	0.1	0.71	0.03	750
X_2	0.2	-0.2	0.71	0.02	619	X_5	0.5	0.2	0.71	0.04	830
X_3	0.3	0	0.71	0.03	677						

left in Figure 2. We moreover let $\xi_1 = 0.02$ and $\xi_2 = 0.03$. The resulting PCFs and cross PCFs are shown in the middle and right plots in Figure 2. In the case $q = 2$

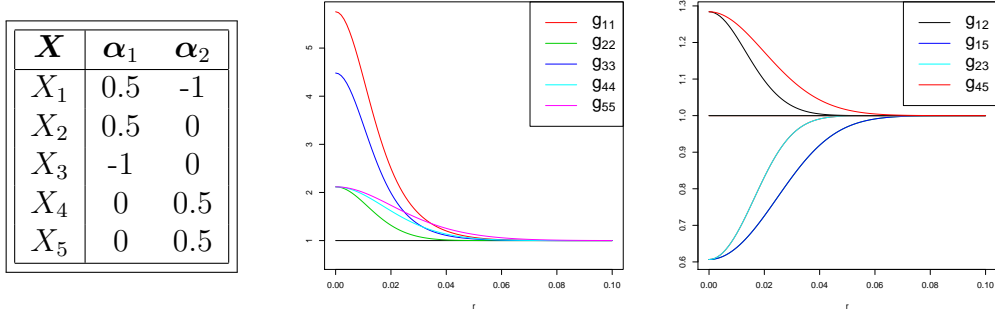


Figure 2: Left: α . Middle: true PCFs. Right: true cross PCFs (note $g_{13} = g_{23}$ and $g_{14} = g_{15}$).

we have a positive spatial dependence between X_1 and X_2 and between X_4 and X_5 , while there is a negative spatial dependence between X_3 and (X_1, X_2) and between X_1 and (X_4, X_5) .

For our second order conditional composite likelihood we specified exponential correlation models for the fields Y_k , $k = 1, \dots, q$ and U_i , $i = 1, \dots, 5$. In practice it is rarely the case that the true correlation models correspond exactly to the specified ones. To reflect this we simulate the Y_k and U_i using Gaussian correlation functions, i.e. $\text{Corr}(Y_k(\mathbf{u}), Y_k(\mathbf{v})) = \exp(-(\|\mathbf{u} - \mathbf{v}\|/\xi_k)^2)$ and $\text{Corr}(U_i(\mathbf{u}), U_i(\mathbf{v})) = \exp(-(\|\mathbf{u} - \mathbf{v}\|/\phi_i)^2)$. Hence the model applied is misspecified for the simulated data. For each setting we generate 100 simulated realizations of \mathbf{X} .

In both settings we select q among the values $0, 1, \dots, 5$, and next, for the chosen q , λ among the values $10, 8, 6, 5, 4, 3, 2, 1, 0.5, 0.25, 0$, using cross validation with $K =$

5 and $L = 10$, and we consider results using both the MIN and the 1-SE approach for the selection of q . We also consider the case where $q = 7$ is fixed in order to assess the effect of regularization in an over-parametrized setting. For the second order conditional composite likelihood we only consider distinct pairs of points \mathbf{u}, \mathbf{v} with $\|\mathbf{u} - \mathbf{v}\| \leq R = 0.1$. All first order parameters are estimated using the approach in Hessellund et al. (2019). The initial parameters for $\boldsymbol{\alpha}$, $\boldsymbol{\xi}$, $\boldsymbol{\sigma}^2$ and $\boldsymbol{\phi}$ are simulated as $\alpha_{ik} \sim \text{Unif}(-0.25, 0.25)$, $\xi_k, \phi_i \sim \text{Unif}(0.01, 0.04)$ and $\sigma_i^2 \sim \text{Unif}(0.4, 0.6)$. The parameter ϵ in the relative function convergence criterion (10) is set to 10^{-5} and the convergence parameters $\tilde{\epsilon}$ and $\tilde{\epsilon}$ for the regularized optimization (15) are set to 10^{-10} .

We measure the performance for each selected model using mean integrated squared error (MISE) aggregated over respectively all PCFs and all cross PCFs, i.e.

$$\text{MISE}_{\text{between}}(\hat{\boldsymbol{\theta}}) = \sum_{i < j} \text{E} \left[\int_{0.01}^{0.1} \left(g_{ij}(r; \hat{\boldsymbol{\theta}}_{ij}) - g_{ij}(r; \boldsymbol{\theta}_{ij}) \right)^2 dr \right], \quad (12)$$

while $\text{MISE}_{\text{within}}(\hat{\boldsymbol{\theta}})$ and $\text{MISE}_{\text{total}}(\hat{\boldsymbol{\theta}})$ are defined in the same way but with sum over $i = j$ or $i \leq j$.

We compare the performance of the proposed method with two non-parametric approaches. For the first approach, referred to as ‘simple’, we estimate the intensity functions non-parametrically using the **spatstat** (Baddeley et al., 2015) procedure **density.ppp** with bandwidths selected using the method introduced in Cronie and van Lieshout (2018). Next the PCFs and cross PCFs are estimated using the **spatstat** procedures **pcfinhom** and **crosspcfinhom** with the intensity functions replaced by the non-parametric estimates. For the PCF and cross PCF estimation we manually specify reasonable bandwidths based on the knowledge of the true PCFs and cross PCFs (note that this is in favor of the non-parametric approach). The second approach is an adaption to the multivariate case of the method proposed in Diggle et al. (2007) (see Section F for details). To measure the performances of the non-parametric approaches we simply replace the fitted parametric cross PCFs in (12) by the non-parametric estimate.

4.1 Five-variate LGCP with zero common latent fields

In the case $q = 0$, the MIN rule only selects the true value $q = 0$ for 1% of the simulated data sets while values of $q = 1, 2, 3$ are selected for 99% of the simulations, see left Table 2. Using the 1-SE rule, $q = 0$ is selected in 77% of the cases and a value of q bigger than 1 is only selected in two cases. The reason that the MIN rule frequently selects q larger than zero may be that in fact neither of the models with $q = 0, \dots, 3$ are severely overparametrized. E.g. with $q = 3$ the in total 15 PCFs and cross PCFs are parametrized using just 25 parameters, i.e. less than 2 parameters on average for each PCF or cross PCF. Hence overfitting that can be detected by the cross validation procedure mainly occurs for $q = 4, 5$. The middle third column in Table 2 (left) shows 95% probability intervals for the selected λ s when $q = 1, 2, 3$ and the last column shows the average percentages of α_{ik} ’s that are estimated to be 0. These columns show that when a larger q is selected then also a larger λ is selected leading to a higher percentage of zeros in the estimated $\boldsymbol{\alpha}$.

Table 2: (Left: true $q = 0$. Right: true $q = 2$) Distribution of q chosen by MIN and 1-SE rules, 95% probability interval for selected λ s, and averages over simulated data sets of percentages of estimated α_{ik} s equal to zero.

q	MIN	1-SE	λ	(% $\alpha_{ik} = 0$)	MIN	1-SE	λ	(% $\alpha_{ik} = 0$)
0	1	77	-	-	0	0	-	-
1	32	21	(0;0.61)	2	2	39	0	0
2	56	2	(0;0.41)	7	60	61	(0;0.38)	1
3	11	0	(0;0.88)	6	36	0	(0;0.25)	0.6
4	0	0	-	-	2	0	0	0
7	-	-	(0;4.52)	52	-	-	(0;2)	26

This makes sense since larger q means more superfluous parameters and hence more need for regularization. In the case $q = 7$ the selected λ s tend to be markedly larger than for the smaller q s up to 3. Also 52% of the α_{ik} are estimated to be zero in the case $q = 7$ while the percentages are quite small for q up to 3. For $q = 1, 2, 3$ the selected λ was zero (meaning no regularization) in 59%, 57%, and 55% of the cases indicating that $q = 1, 2, 3$ already leads to a rather sparse setup and explaining the small percentages of α_{ik} estimated to be zero. Figure 3 shows the average of $\overline{CV}(q, 0)$ over all simulated data sets and confirms that the CV scores are quite similar across different q .

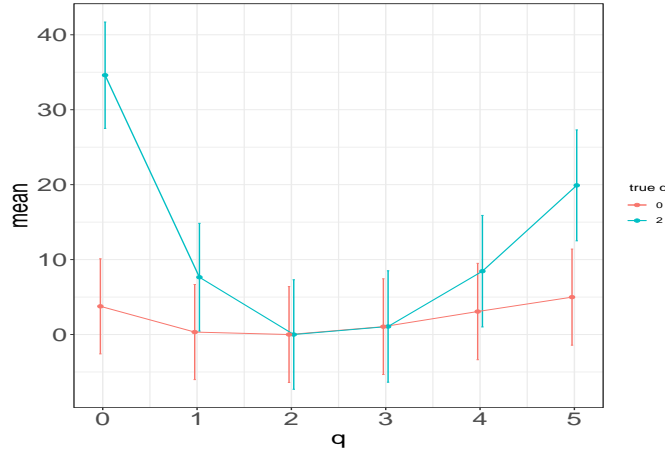


Figure 3: Averages over simulated data sets of $\overline{CV}(q, 0)$ scores with minimum average CV-score subtracted. The bars show the average of the standard errors $SE(q, 0)$ obtained for $\overline{CV}(q, 0)$ for each simulated data set. Red is for $q = 0$ while blue is for $q = 2$.

Figure 4 shows means and 95% pointwise probability intervals for estimates of a subset of the PCFs and cross PCFs obtained for the simulated data sets with q selected among 0, 1, 2, 3, 4, 5 using either MIN or 1-SE and with $\lambda = 0$. We only show estimates with no regularization since the regularized estimates are very similar. The means are quite similar for MIN and 1-SE and the MIN and 1-SE estimates are close to unbiased for the cross PCFs, while a moderate bias is present for the PCF. This bias is not unexpected as we specify the wrong parametric model. However, the simple non-parametric estimates are strongly biased in all cases.

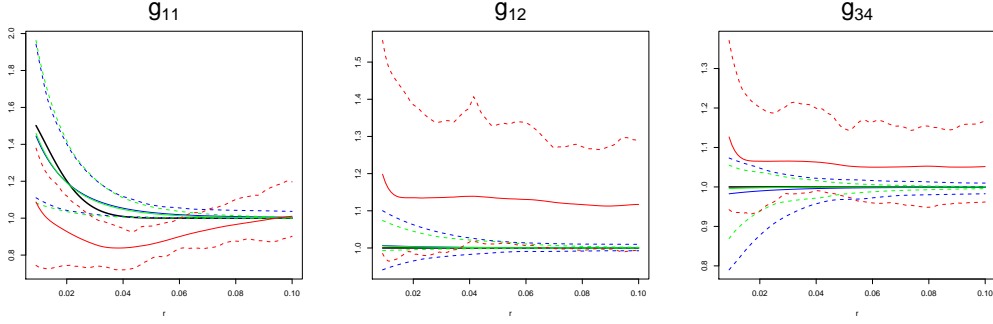


Figure 4: (true $q = 0$) Blue, green and red solid lines indicate pointwise means of estimates for selected cross PCFs using MIN, 1-SE, or simple non-parametric estimation. The dotted lines indicate the corresponding 95% pointwise probability intervals. Black solid lines indicate true cross PCFs.

Table 3: MISE using $(q_{\min}, 0)$, (q_{\min}, λ) , $(q_{1-SE}, 0)$, simple, or Diggle’s non-parametric approach when true $q = 0$.

	$(q_{\min}, 0)$	(q_{\min}, λ)	$(q_{1-SE}, 0)$	simple	Diggle
$MISE_{\text{total}}$	$3.77 \cdot 10^{-4}$	$3.78 \cdot 10^{-4}$	$3.81 \cdot 10^{-4}$	$2.22 \cdot 10^{-3}$	$2.63 \cdot 10^{-3}$
$MISE_{\text{within}}$	$1.02 \cdot 10^{-3}$	$1.02 \cdot 10^{-3}$	$1.11 \cdot 10^{-3}$	$4.58 \cdot 10^{-3}$	$3.36 \cdot 10^{-3}$
$MISE_{\text{between}}$	$5.45 \cdot 10^{-5}$	$5.34 \cdot 10^{-5}$	$2.01 \cdot 10^{-5}$	$1.04 \cdot 10^{-3}$	$2.27 \cdot 10^{-3}$

Table 3 gives total, within and between MISEs with different strategies for choosing (q, λ) and for the two non-parametric approaches. The non-parametric approaches are clearly outperformed by the semi-parametric method. The results for MIN with $\lambda = 0$ or λ selected are very similar and also similar to 1-SE in case of $MISE_{\text{within}}$. However, $MISE_{\text{between}}$ for cross PCFs is more than twice as big for MIN compared to 1-SE. This is not so surprising since 1-SE chooses the true $q = 0$ most of the time while MIN tends to choose larger values of q . The between MISEs are on the other hand on a much smaller scale than the within MISEs.

4.2 Five-variate LGCP with two common latent fields

In case of $q = 2$ both MIN and 1-SE performs quite well in the sense that the chosen q ’s differ at most by one from the true q in 98% (MIN) or in 100% (1-SE) of the cases and the true $q = 2$ is chosen in 60% (MIN) or 61% (1-SE) of the cases. The λ column in Table 2 (right) shows 95% probability intervals for the selected λ s. For $q = 1, 4$ the cross validation always selected $\lambda = 0$. The selected λ s for $q = 2, 3$ are in general small and 80% ($q = 2$) or 95% ($q = 3$) of the λ s were selected to be zero. These results indicate that regularization is not pertinent in this case where the true α is not particularly sparse. Also the percentages of α_{ik} estimated to be zero are very small for $q = 1, 2, 3, 4$. In case of the overparametrized model $q = 7$ we on the other hand do see an effect of regularization with larger selected λ s and on average 26% of the α_{iks} estimated to be zero.

Figure 5 shows means and 95% probability intervals for selected estimated PCFs and cross PCFs obtained with MIN or 1-SE without regularization. In both cases

Table 4: MISE using $(q_{\min}, 0)$, (q_{\min}, λ) , $(q_{1-\text{SE}}, 0)$, the simple or Diggle non-parametric approach when true $q = 2$.

	$(q_{\min}, 0)$	(q_{\min}, λ)	$(q_{1-\text{SE}}, 0)$	simple	Diggle
$\text{MISE}_{\text{total}}$	$1.64 \cdot 10^{-3}$	$1.64 \cdot 10^{-3}$	$1.65 \cdot 10^{-3}$	$7.25 \cdot 10^{-3}$	$4.91 \cdot 10^{-3}$
$\text{MISE}_{\text{within}}$	$4.43 \cdot 10^{-3}$	$4.42 \cdot 10^{-3}$	$4.40 \cdot 10^{-3}$	$2.04 \cdot 10^{-2}$	$8.63 \cdot 10^{-3}$
$\text{MISE}_{\text{between}}$	$2.43 \cdot 10^{-4}$	$2.43 \cdot 10^{-4}$	$2.71 \cdot 10^{-4}$	$6.76 \cdot 10^{-4}$	$3.05 \cdot 10^{-3}$

MIN and 1-SE produce some bias for the PCFs, which is expected as we specify the wrong model. As in the case $q = 0$, the non-parametric estimates are more biased than the semi-parametric estimates.

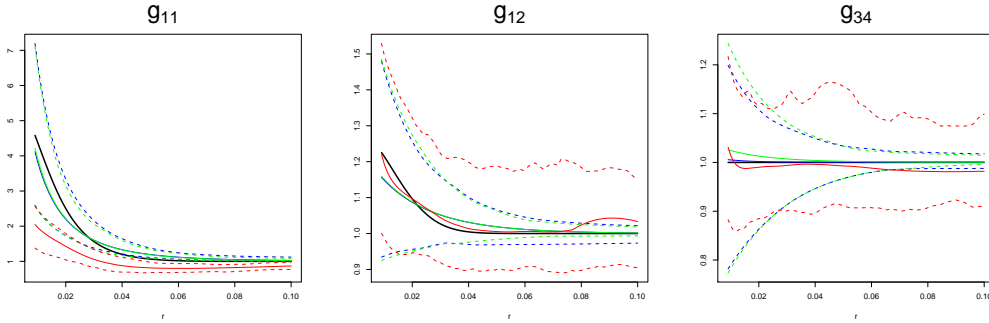


Figure 5: (true $q = 2$) Blue, green and red solid lines indicate pointwise means of estimates for selected cross PCFs using MIN, 1-SE, or simple non-parametric estimation. The dotted lines indicate the corresponding 95% pointwise probability intervals. Black solid lines indicate true cross PCFs.

Table 4 shows that MIN and 1-SE perform very similar regarding MISE. In case of $\text{MISE}_{\text{between}}$, MIN and 1-SE are somewhat better than the simple approach but much better than Diggle’s approach. On the other hand, MIN and 1-SE are somewhat better than Diggle’s approach but much better than the simple approach in terms of $\text{MISE}_{\text{within}}$. Overall ($\text{MISE}_{\text{total}}$) the semi-parametric method outperforms the non-parametric methods.

5 Data examples

In the following we apply our new methodology to point patterns of cells in tumor tissue and crime scenes in Washington DC.

5.1 Lymph node metastasis

Figure 6 shows a fluorescence image of a lymph node metastasis as well as point patterns of locations of four types of cells extracted from the image using machine learning techniques. The four types of cells (with abbreviated names and numbers of cells in parantheses) are Hypoxic tumor cells (Hypoxic, 11733), Normoxic tumor cells (Normoxic, 18469), Stroma cells (Stroma, 6015), and Cytotoxic T-lymphocytes (CD8, 1466). For better visualization we only show random subsets obtained by

independent thinnings of the points. Our aim is to characterize the point patterns in terms of their intensity functions and their PCFs and cross PCFs.

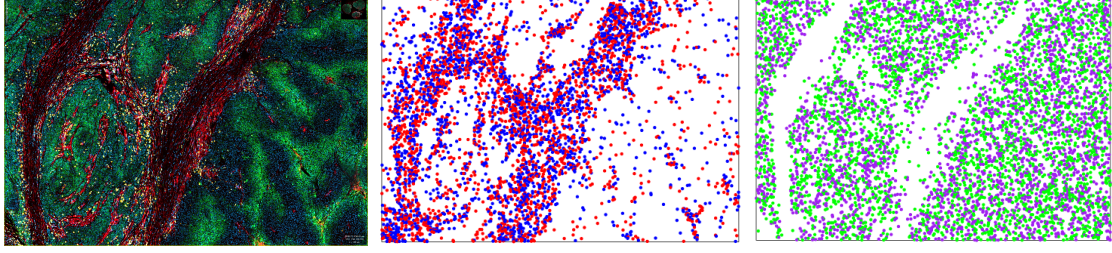


Figure 6: Left: fluorescence image of a lymph node metastasis. Middle: bivariate point pattern of CD8 (blue) and 50% independently thinned Stroma (red) cells. Right: bivariate point pattern of 80% independently thinned Hypoxic (purple) and 80% independently thinned Normoxic (green) cells (data kindly provided by Arnulf Mayer, Dept. of Radiation Oncology, University Medical Center, Mainz, Germany).

Figure 7 shows non-parametric estimates of the intensity functions for the four point patterns. These plots show a strong segregation between the patterns of Stroma and CD8 cells versus the tumor cells. In the following we study the more subtle variation within the bivariate point patterns of Stroma and CD8 respectively Normoxic and Hypoxic. There are no spatial covariates available for this data set so the in-

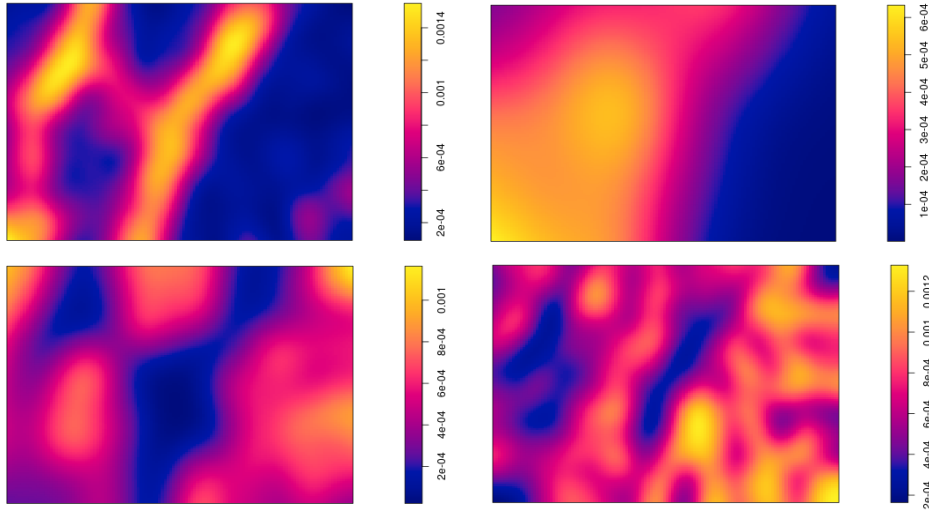


Figure 7: Kernel estimates of the intensity functions for Stroma (upper left), CD8 (upper right), Hypoxic (lower left) and Normoxic (lower right) with bandwidths 121.2, 359.5, 173.9 and 115.7, respectively.

tensity functions will be proportional to the common component $\rho_0(\cdot)$ both for the pairs Stroma,CD8 and Normoxic,Hypoxic. Since the point patterns are of high cardinality we reduce computing time by working with independent thinnings of the point patterns. The PCFs and cross PCFs are invariant to independent thinning while the intensity functions are only changed by a multiplication with the thinning probability. In the following we present a detailed analysis of the Stroma-CD8 point

Table 5: Parameter estimates for Stroma and CD8 for $q = 1$.

	$\hat{\alpha}$	$\hat{\xi}$	$\hat{\sigma}$	$\hat{\phi}$		$\hat{\alpha}$	$\hat{\xi}$	$\hat{\sigma}$	$\hat{\phi}$
Stroma	0.52	63.4	0.32	97.7	CD8	-0.52	63.4	0.78	193.6

pattern. The analysis for the Normoxic-Hypoxic tumor cells is quite similar and is presented in Section G.

5.1.1 Stroma and CD8

For Stroma and CD8 we use all CD8 points and independently thin the Stroma points with a thinning probability of 50%. The point patterns clearly show some large scale trends (Figure 7) that are not easily fitted by simple parametric models. We instead assume the model (3), choose CD8 as the baseline, and following Hessellund et al. (2019) estimate $\beta = (\beta_{\text{Str}}, \beta_{\text{CD8}})^\top = (\gamma_{\text{Str}} - \gamma_{\text{CD8}}, \gamma_{\text{CD8}} - \gamma_{\text{CD8}})^\top$ by $\hat{\beta}_{\text{Str}} = \log(3007/1466) = 0.72$ and $\hat{\beta}_{\text{CD8}} = 0$. We next choose q among the values $\{0, 1, 2\}$ using a 5-fold cross validation as described in Section 3.3, where we resample $L = 10$ times. We choose the maximal interpoint distance R for pairs of points to be 400 μm which corresponds to approximately 15% of the largest observation window side length. According to the left panel in Figure 8 we choose $q = 1$ that minimizes the

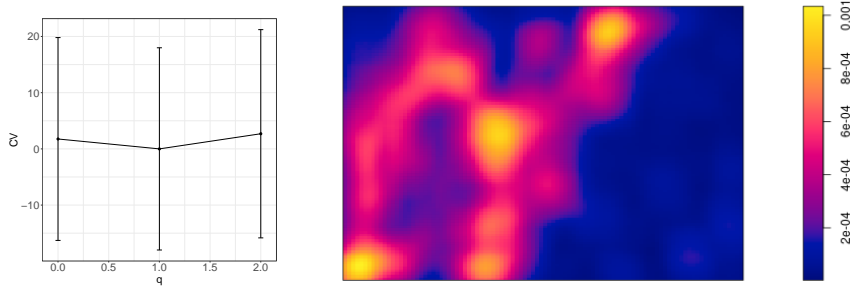


Figure 8: Left: CV-scores (minus minimum CV-score) with standard errors. Right: non-parametric estimate of ρ_0 with bandwidth = 194.5.

cross validation score. The right panel in Figure 8 shows a non-parametric estimate of ρ_0 using the estimator introduced in Hessellund et al. (2019) with bandwidth chosen as described in Section E.

According to the parameter estimates in Table 5 and the resulting PCFs and cross PCFs shown in the left panel of Figure 9 both Stroma and CD8 are randomly clustered point processes. The clustering is partly negatively correlated (cf. $\hat{\alpha}$ and the fitted cross PCF in Figure 9) and partly independent (cf. $\hat{\sigma}$) between Stroma and CD8. The strongest clustering is found for CD8 due to the higher value of $\hat{\sigma}_{\text{CD8}}$ than $\hat{\sigma}_{\text{Str}}$, see also the fitted PCFs in Figure 9.

The total estimated variances for the log random intensity functions of Stroma and CD8 are rather moderate, respectively 0.37 and 0.88, while the empirical variance of $\log \hat{\rho}_0$ over the observation window is 1.15. In this sense, the majority of the variation in the random intensity functions (especially for Stroma) is explained by ρ_0 .

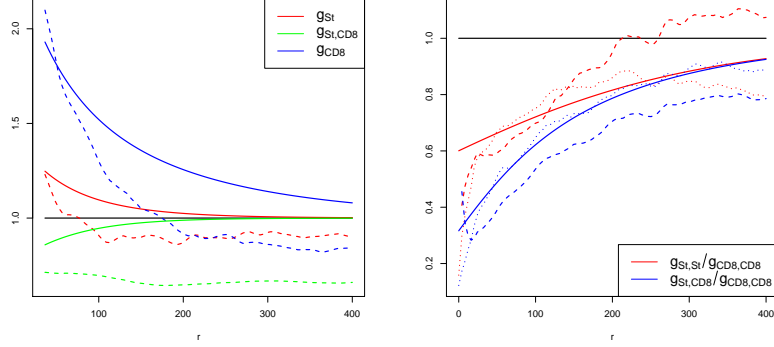


Figure 9: Left: estimated (cross) PCFs using the semi-parametric model (solid) and simple approach (dashed). Right: estimated (cross) PCF ratio using semi-parametric model (solid), simple approach (dashed) and consistent approach (dotted).

Following Section 3.4, the right panel in Figure 9 compares semi-parametric estimates of cross PCF ratios $g_{\text{Str}}/g_{\text{CD8}}$ and $g_{\text{Str,CD8}}/g_{\text{CD8}}$ with the non-parametric estimates introduced in Hessellund et al. (2019). The agreement seems reasonable and this is confirmed by global envelope p -values of 0.05 in case of $g_{\text{Str}}/g_{\text{CD8}}$ and 0.09 for $g_{\text{Str,CD8}}/g_{\text{CD8,CD8}}$, see also the global envelope plots in Section H.

Figure 9 (left) also shows simple non-parametric PCF and cross PCF estimates which are generally smaller than the semi-parametric estimates. In particular, the non-parametric estimate of the cross PCF suggests a strong negative correlation between Stroma and CD8 for all spatial lags considered. As discussed in Shaw et al. (2020) this might be due to that the selected bandwidths imply too little smoothing in the non-parametric intensity estimates (upper plots in Figure 7). Figure 9 (right) further shows that the simple estimates of cross PCF ratios deviate more from the consistent non-parametric estimates than the semi-parametric estimates.

5.2 Washington DC street crimes

It is of great interest for criminologists and police authorities to study the spatial patterns of crime scenes since this can lead to better understanding of factors affecting crime and more efficient policing strategies. In this section we focus on the spatial correlation between six common types of street crimes committed in Washington DC in January and February 2017. These are extracted from a larger data set publicly available from <http://opendata.dc.gov/datasets/>. The six types of crimes with numbers in parantheses are 1) Burglary (259), 2) Assault with weapon (332), 3) Motor vehicle theft (335), 4) Theft from automobile (1832), 5) Robbery (366), and 6) Other theft (2254). This data set has previously been considered by Hessellund et al. (2019) who focused on the dependency of the street crime intensity functions on spatial covariates using the model (3). In the following we focus on the second order properties as described by the PCFs and cross PCFs. We refer to Hessellund et al. (2019) for more details regarding the covariates and the fitted intensity functions.

We apply the regularized estimation approach described in Sections 3.2-3.3 where

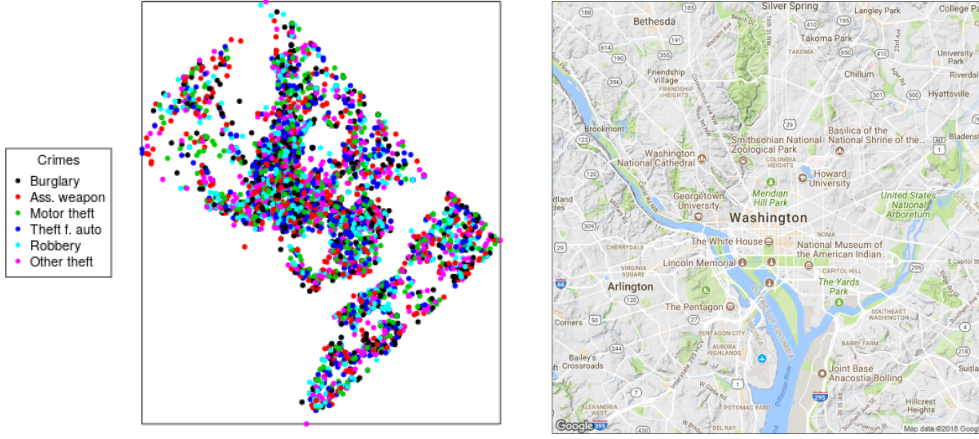


Figure 10: Left: street crimes locations ($n = 5378$). Right: a map of Washington DC.

we first determine q using cross validation without regularization and next, for the chosen q , use another cross validation to select the regularization parameter λ to potentially obtain a sparse submodel for the chosen q . For the cross validation we use $K = 5$ and $L = 10$ and choose q among $\{0, 1, \dots, 5\}$ and λ in the set $\{100, 80, 60, 50, 40, 30, 20, 10, 5, 2.5, 1, 0.25, 0\}$. For the second order composite likelihood we use $R = 1000$ meters.

The left panel in Figure 11 shows cross validation scores for each q , where the 1-SE criterion leads to choosing $q = 0$ while MIN chooses $q = 1$. The middle panel show CV-scores for each λ with $q = 1$ where the minimum is obtained for $\lambda = 0$. The right panel in Figure 11 shows a non-parametric estimate of ρ_0 using the estimator described in Hessellund et al. (2019) with bandwidth chosen as described in Section E. In the following we focus on the results with $q = 1$ and $\lambda = 0$. Hence we obtain an estimate of α without any regularization.

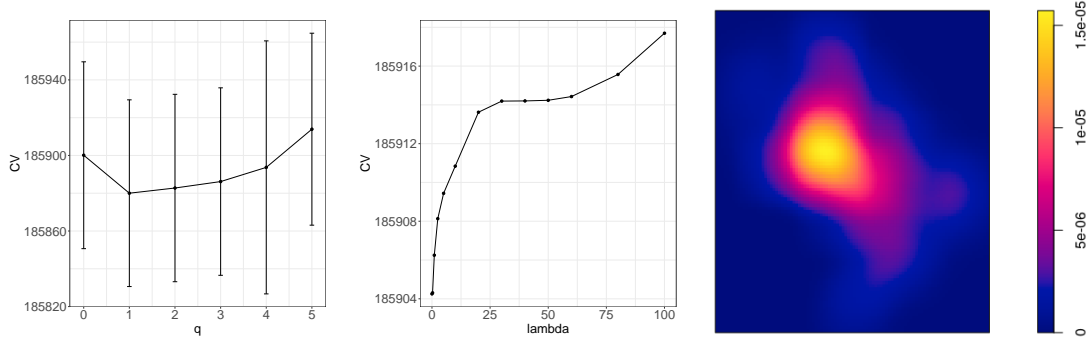


Figure 11: Left: CV-score for q with one standard error bars. Middle: CV-score for λ given $q = 1$. Right: non-parametric estimate of ρ_0 with bandwidth 2654 meters.

The parameter estimates for each street crime are given in Table 6 except for the common latent field correlation scale parameter estimate which is $\hat{\xi} = 102.5$. The σ_i estimates are small to moderate for the first five crimes while the estimate $\hat{\sigma}_6$ for Other theft is about two times larger than the other σ_i estimates. Regarding the latent field Y_1 the α_{i1} estimates are pretty small for Assault, Vehicle theft, Theft

Table 6: Table of parameter estimates for each street crime for $(q, \lambda) = (1, 0)$. Last two columns show estimates of α_l , $l = 1, 2$ with $(q, \lambda) = (2, 2.5)$.

Crime type	$\hat{\alpha}$	$\hat{\sigma}$	$\hat{\phi}$	$\hat{\alpha}_{.1}$	$\hat{\alpha}_{.2}$
Burglary	0.78	0.50	245.8	0	0.76
Assault	-0.12	0.51	457.5	0	-0.09
Vehicle Theft	0.49	0.14	20.5	0	0.47
Theft F. Auto	0.09	0.58	2483.1	0	0.08
Robbery	-0.30	0.53	485.2	0	-0.26
Other theft	-0.93	0.96	20.5	0	-0.97

from auto, and Robbery while α_{11} for Burglary and α_{61} for Other theft have fairly large estimates 0.78 and -0.93 . The resulting estimated PCFs and cross PCFs are shown in the left and middle panels of Figure 12. The overall conclusion is that most crimes are moderately clustered except for Burglary and Other theft with strongest clustering for Other theft. Also the cross dependencies seem fairly weak except for pairs involving the crimes Burglary, Vehicle theft and Other theft (crimes 1,3,6) with Burglary and Vehicle theft being positively correlated and Burglary and Other theft being negatively correlated. The interpretation of these results is that except for moderate random fluctuations, the spatial patterns of Assault, Vehicle theft, Theft from auto and Robbery are quite well described by their intensity functions depending on the common factor ρ_0 as well as covariate effects. On the other hand, the random intensity functions for Burglary and Other theft seem subject to more pronounced deviations from the intensity functions and these deviations are negatively correlated. In other words if a cluster of Burglaries not explained by the intensity function is present in a certain area then there tends to be less Other theft committed in the same area and vice versa.

We also tried out $q = 2$ for which the cross validation score is quite close to the one for $q = 1$. For $q = 2$ the cross validation selected $\lambda = 2.5$. The last columns in Table 6 show the estimate of α obtained with $(q, \lambda) = (2, 2.5)$. The lasso regularization has shrunk $\hat{\alpha}_{.1}$ to $\mathbf{0}$, while the estimate of $\alpha_{.2}$ is quite similar to the estimate of $\alpha_{.1}$ for $q = 1$. In view of this, one may argue that the lasso regularization makes our estimation approach more robust, since a too large selected q can be counterbalanced by regularization on α with a $\lambda > 0$.

Quite different conclusions are obtained with the simple non-parametric analysis. Figure 12 shows that the non-parametric estimates of the PCFs and cross PCFs are all considerably above the reference value 1 which would imply strong clustering within and between the different types of crime. These results may well be explained by bias of the non-parametric estimates.

For model assessment we consider global envelope tests based on differences between semi-parametric and consistent non-parametric estimates for all 20 ratios g_{ij}/g_{66} , $1 \leq i \leq j \leq 6$, $(i, j) \neq (6, 6)$. The p -values obtained are between 0.089 and 0.624 and hence do not provide evidence against our model. Some representative global envelope plots for the differences are shown in Section I.

We finally consider an explorative analysis focusing on patterns in the common latent process Y_1 . We define ‘residuals’ $\Delta \log \Lambda_i(\mathbf{u})$ by $\log \Lambda_i(\mathbf{u}) - \mu_i - \beta_i^T \mathbf{z}(\mathbf{u}) -$

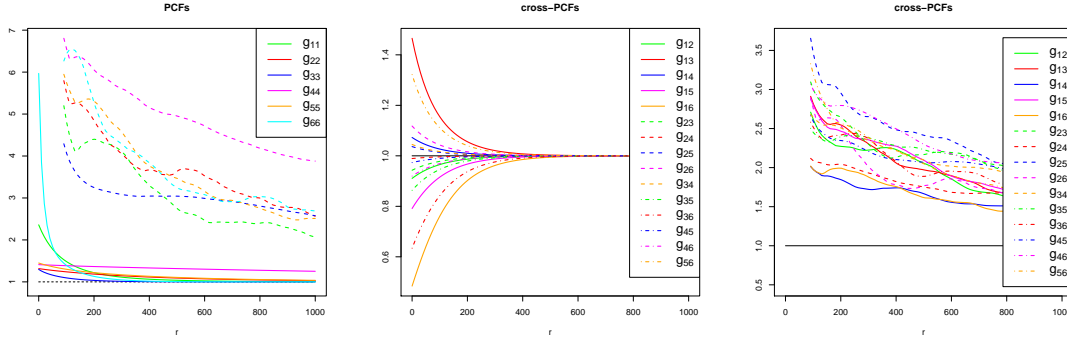


Figure 12: Left: semi-parametric (solid) and simple non-parametric (dashed) estimates of PCFs for $(q, \lambda) = (1, 0)$. Middle: semi-parametric estimates of cross PCFs for $(q, \lambda) = (1, 0)$. Right: simple non-parametric estimates of cross PCFs.

$\frac{1}{p} \sum_{l=1}^p [\log \Lambda_l(\mathbf{u}) - \mu_l - \beta_l^\top \mathbf{z}(\mathbf{u})]$. Due to the sum-to-zero constraint on α we obtain $\Delta \log \Lambda_i(\mathbf{u}) = \alpha_{i1} Y_1(u) + \sigma_i U_i - \frac{1}{p} \sum_{l=1}^p \sigma_l U_l(\mathbf{u})$. Estimating $\Delta \log \Lambda_i$ by replacing Λ_i by a kernel estimate and the parameters by their conditional likelihood estimates, we obtain $\hat{Y}_1(u) = (\hat{\alpha}^\top \hat{\alpha})^{-1} \hat{\alpha} [\hat{\Delta} \log \Lambda_1(u), \dots, \hat{\Delta} \log \Lambda_p(u)]^\top$. The left plot in Figure 13 shows \hat{Y}_1 where the Λ_i are estimated by kernel smoothing using a bandwidth of 3 km. There is some resemblance between $\hat{Y}_1(\mathbf{u}; h)$ and the spatial distribution of median income shown in the middle plot of Figure 13. Log median income is included as a covariate in the regression model for the log intensity so it may be the case that $\hat{Y}_1(\mathbf{u})$ reflects nonlinear effects of the financial status of a neighborhood, cf. the right plot in Figure 13.

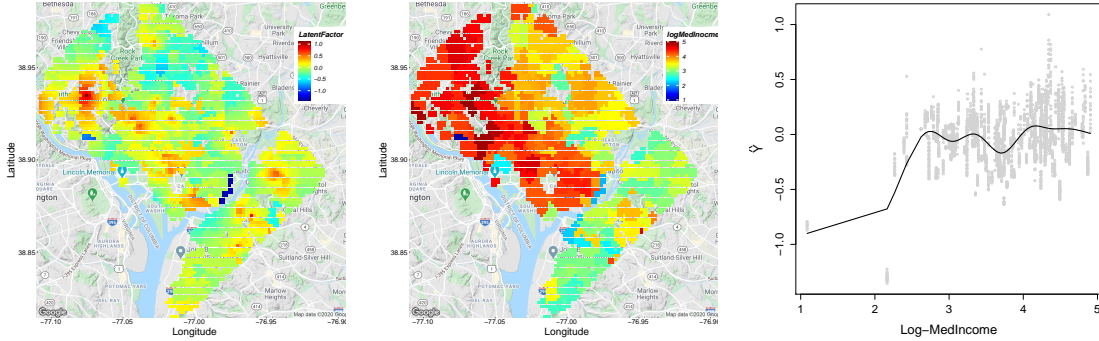


Figure 13: Left: latent factor \hat{Y}_1 . Middle: log median income within census tracts. Right: \hat{Y}_1 versus log median income.

6 Conclusion

The methodology introduced in this paper provides a major step forward regarding second order analysis of multivariate point processes with complex intensity functions. Existing approaches (such as simple non-parametric estimation or the approach in Diggle et al., 2007) rely on estimating the intensity functions using

kernel estimators and this tends to result in strong bias and/or large variance for subsequent estimation of PCFs and cross PCFs. In contrast, in the context of the model (3), our approach circumvents the need to estimate the complex unknown intensity function factor ρ_0 and the resulting PCF and cross PCFs appear to be close to unbiased according to our simulation studies. For the data examples considered we obtain simple and interpretable models that may result in better understanding of the interplay between respectively cells in tumors and different types of crimes.

A limitation of our approach, shared with existing methods, is that we have not provided confidence intervals for parameter estimates or confidence bands for estimated PCFs or cross PCFs. One topic for further research would be to establish asymptotic results for parameter estimates within the framework of estimating function inference. This was done by Hessellund et al. (2019) regarding inference for the intensity function but the current problem of inferring cross PCFs entail considerable additional theoretical difficulties.

The impact of using regularization was not very strong in our simulation studies when moderate values of q were considered. However, the crimes data example indicates that the use of regularization may add robustness to the estimation procedure if a too large q is selected.

Acknowledgements

We thank Arnulf Mayer, Dept. of Radiation Oncology, University Medical Center, Mainz, Germany, for providing the fluorescence image and the point pattern data. Kristian B. Hessellund and Rasmus Waagepetersen were supported by The Danish Council for Independent Research — Natural Sciences, grant DFF - 7014-00074 ‘Statistics for point processes in space and beyond’, and by the Centre for Stochastic Geometry and Advanced Bioimaging, funded by grant 8721 from the Villum Foundation.

A Conditional probability and likelihood

Define $X^{\text{pooled}} = \cup_{i=1}^p X_i$ with intensity function $\sum_i \rho_i$ and second order joint intensity $\sum_{l,k} \rho_{lk}$. Define further the measure

$$C(A \times B \times \{i\} \times \{j\}) = \mathbb{E} \sum_{\substack{\neq \\ \mathbf{u}, \mathbf{v} \in X^{\text{pooled}}}} 1[\mathbf{u} \in A, \mathbf{v} \in B, \mathbf{u} \in X_i, \mathbf{v} \in X_j]$$

By Radon-Nikodym’s theorem,

$$C(A \times B \times \{i\} \times \{j\}) = \int_{A \times B} p_{ij}(\mathbf{u}, \mathbf{v}) \left[\sum_{l,k} \rho_{lk}(\mathbf{u}, \mathbf{v}) \right] d\mathbf{u} d\mathbf{v},$$

where for almost all (\mathbf{u}, \mathbf{v}) , $p_{ij}(\mathbf{u}, \mathbf{v})$ is a probability function on $\{1, \dots, p\} \times \{1, \dots, p\}$. This follows because $C(\cdot \times \cdot \times \{i\} \times \{j\})$ is absolutely continuous with respect to

the second order factorial measure

$$\alpha(A \times B) = \mathbb{E} \sum_{\substack{\neq \\ \mathbf{u}, \mathbf{v} \in X^{\text{pooled}}}} 1[\mathbf{u} \in A, \mathbf{v} \in B]$$

of X^{pool} which has density $\sum_{l,k} \rho_{lk}$. It is then natural to interpret $p_{ij}(\mathbf{u}, \mathbf{v})$ as the conditional (Palm) probability that $\mathbf{u} \in X_i, \mathbf{v} \in X_j$ given that $\mathbf{u}, \mathbf{v} \in X^{\text{pool}}$ since $\sum_{l,k} \rho_{lk}(\mathbf{u}, \mathbf{v}) d\mathbf{u} d\mathbf{v}$ is the ‘probability’ that X^{pool} ‘has points at \mathbf{u} and \mathbf{v} ’. On the other hand,

$$C(A \times B \times \{i\} \times \{j\}) = \int_{A \times B} \rho_{ij}(\mathbf{u}, \mathbf{v}) d\mathbf{u} d\mathbf{v}.$$

Thus we obtain (6).

Another way to arrive at (6) is to define point processes $X_{ij} = \{(\mathbf{u}, \mathbf{v}) | \mathbf{u} \in X_i, \mathbf{v} \in X_j, \mathbf{u} \neq \mathbf{v}\}$ with intensity functions $\rho_{ij}(\mathbf{u}, \mathbf{v})$. We can further define the union $\tilde{X}^{\text{pool}} = \cup_{i,j} X_{ij}$ with intensity function $\sum_{k,l} \rho_{kl}$. If we now condition on \tilde{X}^{pool} and consider a point $(\mathbf{u}, \mathbf{v}) \in \tilde{X}^{\text{pool}}$, then (6) is the conditional probability that this point comes from X_{ij} . We could also define \tilde{X}^{pool} as $\cup_{i \leq j} X_{ij}$ in which case we would get the conditional probabilities

$$q_{ij}(\mathbf{u}, \mathbf{v}) = \frac{\rho_{ij}(\mathbf{u}, \mathbf{v})}{\sum_{l \leq k} \rho_{lk}(\mathbf{u}, \mathbf{v})}. \quad (13)$$

Remark A.1. *An important property of (7) is that the score function is unbiased, see Lemma B.1. For this to hold it is crucial that when we sum over all l, k in the denominator of (6) we also use product over all i, j in (7). Alternatively, using (13) we could define*

$$L(\boldsymbol{\theta}) = \prod_{i \leq j} \prod_{\substack{\neq \\ \mathbf{u} \in X_i \cap W \\ \mathbf{v} \in X_j \cap W \\ \|\mathbf{u} - \mathbf{v}\| \leq R}} q_{ij}(\mathbf{u}, \mathbf{v}; \boldsymbol{\theta}). \quad (14)$$

In this case a pair $\{\mathbf{u}, \mathbf{v}\}$ with $\mathbf{u} \in X_i$ and $\mathbf{v} \in X_j$ only appears once for $i \neq j$ since the sum is now only over $i \leq j$. However, a pair $\mathbf{u} \neq \mathbf{v} \in X_i$ will contribute twice to the likelihood. We tried out the two alternatives (7) and (14) on a number of data sets and got very similar estimates.

Remark A.2. *Note that if an ordered pair (\mathbf{u}, \mathbf{v}) appears in the product in (7) then so does (\mathbf{v}, \mathbf{u}) . Hence in a practical implementation we may restrict the product to $i \leq j$ and if $i = j$ only include unordered pairs $\{\mathbf{u}, \mathbf{v}\}$ with $\mathbf{u} \neq \mathbf{v} \in X_i$. We can finally square to get (7).*

B Theoretical results concerning conditional composite likelihood score and Hessian

In this section $\boldsymbol{\theta}^*$ denotes the parameter vector for which the data is generated.

Lemma B.1. *The score function $e(\boldsymbol{\theta}) = \nabla_{\boldsymbol{\tau}} l_{-}(\boldsymbol{\theta})$ is unbiased meaning $\mathbb{E}[e(\boldsymbol{\theta}^*)] = 0$.*

Proof.

$$\begin{aligned}
\mathbb{E}[e(\boldsymbol{\theta}^*)] &= \mathbb{E} \left[\sum_{i,j} \sum_{\substack{\mathbf{u} \in X_i \cap W \\ \mathbf{v} \in X_j \cap W}}^{\neq} \left(\frac{\sum_{k,l} \nabla_{\boldsymbol{\tau}} \rho_{kl}(\mathbf{u}, \mathbf{v}; \boldsymbol{\theta}_{kl}^*)}{\sum_{k,l} \rho_{kl}(\mathbf{u}, \mathbf{v}; \boldsymbol{\theta}_{kl}^*)} - \frac{\nabla_{\boldsymbol{\tau}} \rho_{ij}(\mathbf{u}, \mathbf{v}; \boldsymbol{\theta}_{ij}^*)}{\rho_{ij}(\mathbf{u}, \mathbf{v}; \boldsymbol{\theta}_{ij}^*)} \right) \right] \\
&= \sum_{i,j} \int_{W^2} \left(\frac{\sum_{k,l} \nabla_{\boldsymbol{\tau}} \rho_{kl}(\mathbf{u}, \mathbf{v}; \boldsymbol{\theta}_{kl}^*)}{\sum_{k,l} \rho_{kl}(\mathbf{u}, \mathbf{v}; \boldsymbol{\theta}_{kl}^*)} - \frac{\nabla_{\boldsymbol{\tau}} \rho_{ij}(\mathbf{u}, \mathbf{v}; \boldsymbol{\theta}_{ij}^*)}{\rho_{ij}(\mathbf{u}, \mathbf{v}; \boldsymbol{\theta}_{ij}^*)} \right) \rho_{ij}(\mathbf{u}, \mathbf{v}; \boldsymbol{\theta}_{ij}^*) d\mathbf{u} d\mathbf{v} \\
&= \int_{W^2} \sum_{k,l} \nabla_{\boldsymbol{\tau}} \rho_{kl}(\mathbf{u}, \mathbf{v}; \boldsymbol{\theta}_{kl}^*) - \sum_{i,j} \nabla_{\boldsymbol{\tau}} \rho_{ij}(\mathbf{u}, \mathbf{v}; \boldsymbol{\theta}_{ij}^*) d\mathbf{u} d\mathbf{v} = \mathbf{0}.
\end{aligned}$$

□

Lemma B.2. *The expected Hessian matrix of $l_-(\boldsymbol{\theta}^*)$ with respect to $\boldsymbol{\tau}$ is given by:*

$$\mathbb{H}(\boldsymbol{\theta}^*) = \int_{W^2} 1_R(\mathbf{u}, \mathbf{v}) \text{Cov}(Z(\mathbf{u}, \mathbf{v}, \boldsymbol{\theta}^*)) \sum_{i,j} \rho_{ij}(\mathbf{u}, \mathbf{v}; \boldsymbol{\theta}^*) d\mathbf{u} d\mathbf{v},$$

where for each \mathbf{u}, \mathbf{v} , $Z(\mathbf{u}, \mathbf{v}, \boldsymbol{\theta}^*)$ denotes a random vector which takes values $\nabla_{\boldsymbol{\tau}} \log \rho_{ij}(\mathbf{u}, \mathbf{v}; \boldsymbol{\theta}^*)$ with probabilities $p_{ij}(\mathbf{u}, \mathbf{v}; \boldsymbol{\theta}^*)$, $i, j = 1, \dots, p$.

Proof. We suppress the arguments \mathbf{u}, \mathbf{v} and $\boldsymbol{\theta}^*$ in order to save space. The Hessian matrix for $l_-(\boldsymbol{\theta})$ is:

$$\begin{aligned}
\frac{\partial}{\partial \boldsymbol{\tau}^T} e(\boldsymbol{\theta}) &= \nabla_{\boldsymbol{\tau}}^2 l_-(\boldsymbol{\theta}) = \\
&\sum_{i,j} \sum_{\substack{\mathbf{u} \in X_i \cap W \\ \mathbf{v} \in X_j \cap W}}^{\neq} \frac{(\sum_{k,l} \nabla_{\boldsymbol{\tau}}^2 \rho_{kl})(\sum_{k,l} \rho_{kl}) - (\sum_{k,l} \nabla_{\boldsymbol{\tau}} \rho_{kl})(\sum_{k,l} \nabla_{\boldsymbol{\tau}}^T \rho_{kl})}{(\sum_{k,l} \rho_{kl})^2} - \\
&\sum_{i,j} \sum_{\substack{\mathbf{u} \in X_i \cap W \\ \mathbf{v} \in X_j \cap W}}^{\neq} \frac{(\nabla_{\boldsymbol{\tau}}^2 \rho_{ij}) \rho_{ij} - (\nabla_{\boldsymbol{\tau}} \rho_{ij})(\nabla_{\boldsymbol{\tau}}^T \rho_{ij})}{\rho_{ij}^2}
\end{aligned}$$

The expected Hessian is then given by:

$$\begin{aligned}
& H(\boldsymbol{\theta}^*) \\
&= \sum_{i,j} \int_{W^2} 1_R \frac{(\sum_{k,l} \nabla_{\boldsymbol{\tau}}^2 \rho_{kl})(\sum_{k,l} \rho_{kl}) - (\sum_{k,l} \nabla_{\boldsymbol{\tau}} \rho_{kl})(\sum_{k,l} \nabla_{\boldsymbol{\tau}}^T \rho_{kl})}{(\sum_{k,l} \rho_{kl})^2} \rho_{ij} dudv - \\
&\quad \sum_{i,j} \int_{W^2} 1_R \frac{(\nabla_{\boldsymbol{\tau}}^2 \rho_{ij}) \rho_{ij} - (\nabla_{\boldsymbol{\tau}} \rho_{ij})(\nabla_{\boldsymbol{\tau}}^T \rho_{ij})}{\rho_{ij}^2} \rho_{ij} dudv \\
&= \int_{W^2} 1_R \sum_{i,j} \frac{(\nabla_{\boldsymbol{\tau}} \rho_{ij})(\nabla_{\boldsymbol{\tau}}^T \rho_{ij})}{\rho_{ij}} - \frac{(\sum_{k,l} \nabla_{\boldsymbol{\tau}} \rho_{kl})(\sum_{k,l} \nabla_{\boldsymbol{\tau}}^T \rho_{kl})}{(\sum_{k,l} \rho_{kl})} dudv \\
&= \int_{W^2} 1_R \left(\sum_{k,l} \rho_{kl} \right) \left(\sum_{i,j} \nabla_{\boldsymbol{\tau}} \log(\rho_{ij}) \nabla_{\boldsymbol{\tau}}^T \log(\rho_{ij}) p_{ij} \right) dudv \\
&\quad - \int_{W^2} 1_R \left(\sum_{k,l} \rho_{kl} \right) \left(\left(\sum_{k,l} \nabla_{\boldsymbol{\tau}} \log(\rho_{kl}) p_{kl} \right) \left(\sum_{k,l} \nabla_{\boldsymbol{\tau}} \log(\rho_{kl}) p_{kl} \right)^T \right) dudv \\
&= \int_{W^2} 1_R \left(\sum_{i,j} \rho_{ij} \right) \text{Cov}(Z(\boldsymbol{\theta}^*)) dudv.
\end{aligned}$$

□

C Quadratic approximation and least squares

Omitting the first term not depending on $\boldsymbol{\tau}$ and letting $K = -H^{-1}(\tilde{\boldsymbol{\tau}})e(\tilde{\boldsymbol{\tau}})$, the quadratic approximation (8) can be rewritten as follows:

$$\begin{aligned}
& (\boldsymbol{\tau} - \tilde{\boldsymbol{\tau}})^T e(\tilde{\boldsymbol{\tau}}) + \frac{1}{2} (\boldsymbol{\tau} - \tilde{\boldsymbol{\tau}})^T H(\tilde{\boldsymbol{\tau}}) (\boldsymbol{\tau} - \tilde{\boldsymbol{\tau}}) \\
&= -(\boldsymbol{\tau} - \tilde{\boldsymbol{\tau}})^T H(\tilde{\boldsymbol{\tau}}) K + \frac{1}{2} (\boldsymbol{\tau} - \tilde{\boldsymbol{\tau}})^T H(\tilde{\boldsymbol{\tau}}) (\boldsymbol{\tau} - \tilde{\boldsymbol{\tau}}) \\
&= \frac{1}{2} (K - (\boldsymbol{\tau} - \tilde{\boldsymbol{\tau}}))^T H(\tilde{\boldsymbol{\tau}}) (K - (\boldsymbol{\tau} - \tilde{\boldsymbol{\tau}})) - \frac{1}{2} K^T H(\tilde{\boldsymbol{\tau}}) K.
\end{aligned}$$

Hence, minimizing (8) is a least squares problem:

$$\hat{\boldsymbol{\tau}} = \arg \min_{\boldsymbol{\tau}} \left(\|H(\tilde{\boldsymbol{\tau}})^{1/2} (K - (\boldsymbol{\tau} - \tilde{\boldsymbol{\tau}}))\|^2 \right) = \arg \min_{\boldsymbol{\tau}} \left(\|Y - X\boldsymbol{\tau}\|^2 \right),$$

where

$$Y = H(\tilde{\boldsymbol{\tau}})^{1/2} (-H(\tilde{\boldsymbol{\tau}})^{-1} e(\tilde{\boldsymbol{\tau}}) + \tilde{\boldsymbol{\tau}}) \quad \text{and} \quad X = H(\tilde{\boldsymbol{\tau}})^{1/2}.$$

D Update of regularized α

Following Shi et al. (2016) we update α by minimizing the augmented Lagrangian object function

$$Q_{\lambda,\mu}(\alpha, \eta) = \frac{1}{2} \|Y - X\alpha\|^2 + \lambda \sum_{i=1}^p \sum_{j=1}^q |\alpha_{ij}| + \eta C\alpha + \frac{\mu}{2} \|C\alpha\|^2,$$

where $\eta \in \mathbb{R}^q$ is the Lagrange multiplier and $\mu > 0$ is a penalty parameter that we set to 1 as in Shi et al. (2016). Letting α^{current} , η^{current} , α^{new} , and η^{new} denote temporary vectors used in the iterative algorithm, we initialize $\alpha^{\text{current}} = \alpha^{(n)}$ and $\eta^{\text{current}} = \mathbf{0}$. We then iterate updates

$$\alpha^{\text{new}} \leftarrow \arg \min_{\alpha} Q_{\lambda,\mu}(\alpha, \eta^{\text{current}}, \pi^{(n)}) \quad \eta^{\text{new}} \leftarrow \eta^{\text{current}} + \mu C\alpha^{\text{new}}.$$

The updating is terminated if for some $\tilde{\epsilon}$ and $\tilde{\tilde{\epsilon}}$,

$$\|\alpha^{\text{new}} - \alpha^{\text{current}}\| < \tilde{\epsilon} \quad \text{and} \quad \|\eta^{\text{new}} - \eta^{\text{current}}\| < \tilde{\tilde{\epsilon}}, \quad (15)$$

in which case $\hat{\alpha} := \alpha^{\text{new}}$. Otherwise $\alpha^{\text{current}} \leftarrow \alpha^{\text{new}}$ and $\eta^{\text{current}} \leftarrow \eta^{\text{new}}$ and a new iteration takes place.

The update leading to α^{new} is conducted using cyclical updating of the entries α_{ij}^{new} in α^{new} . The update of the ij th entry is

$$\begin{aligned} c_1 &\leftarrow X_{\cdot ij}^T \left(Y - \sum_{lk \neq ij} X_{\cdot lk} \alpha_{lk}^{\text{new}} \right) \\ c_2 &\leftarrow \mu \left(\sum_{lk \neq ij} \alpha_{lk}^{\text{new}} C_{lk}^T C_{\cdot ij} + C_{\cdot ij}^T \eta / \mu \right) \\ \alpha_{ij}^{\text{new}} &\leftarrow \frac{S(c_1 - c_2, \lambda)}{X_{\cdot ij}^T X_{\cdot ij} + \mu C_{\cdot ij}^T C_{\cdot ij}}, \end{aligned} \quad (16)$$

where $X_{\cdot ij}$ and $C_{\cdot ij}$ are the columns of X and C corresponding to α_{ij} (i.e. when α is laid out columnwise) and $S(\cdot, \cdot)$ is a soft-thresholding operator given by:

$$S(c, \lambda) = \begin{cases} c - \lambda & \text{if } c > 0 \text{ and } \lambda < |c| \\ c + \lambda & \text{if } c < 0 \text{ and } \lambda < |c| \\ 0 & \text{if } \lambda > |c|. \end{cases}$$

Algorithm 2 gives an overview of the regularized cyclical block descent algorithm.

E Bandwidth selection for ρ_0

Following Hessellund et al. (2019) we can estimate ρ_0 using the semi-parametric kernel estimator:

$$\hat{\rho}_0(\mathbf{u}) = \frac{1}{p} \sum_{i=1}^p \sum_{\mathbf{v} \in X_i} \exp(-\hat{\beta}_i^T \mathbf{z}(\mathbf{v})) \frac{k((\mathbf{u} - \mathbf{v})/b)}{b^d c_b(\mathbf{v})}, \quad (17)$$

Algorithm 2 Regularized cyclical block descent algorithm

- 1: Simulate initial parameters $\hat{\alpha}^{(0)}, \hat{\xi}^{(0)}, \hat{\sigma}^{2(0)}$ and $\hat{\phi}^{(0)}$
 - 2: $n := 0$
 - 3: **repeat**
 - 4: $\tilde{\alpha} := \alpha^{(n)}, \tilde{\xi} := \xi^{(n)}, \tilde{\sigma}^2 := \sigma^{2(n)}$ and $\phi := \phi^{(n)}$
 - 5: update $\tilde{\alpha}$ using augmented Lagrangian method followed by line search
 - 6: update $\tilde{\xi}, \tilde{\sigma}^2$ and $\tilde{\phi}$ in turn using (9) followed by line search
 - 7: $\alpha^{(n+1)} := \tilde{\alpha}, \xi^{(n+1)} := \tilde{\xi}, \sigma^{2(n+1)} := \tilde{\sigma}^2$, and $\phi^{(n+1)} := \tilde{\phi}$
 - 8: $n := n + 1$
 - 9: **until** relative convergence for object function (11)
 - 10: **return** $\hat{\theta} = \theta^{(n)}$
-

where k is a d -dimensional kernel, b is the bandwidth, and $c_b(v) = \int_W k(\mathbf{u} - \mathbf{v}) d\mathbf{u}$ is an edge correction factor.

We suggest to choose the bandwidth according to a criterion inspired by Cronie and van Lieshout (2016) who consider the squared difference between the observation window area and an estimate (depending on the bandwidth) of this area. However, exact knowledge of the observation window area may not always be available (this is e.g. the case for the crimes data where the observation window depends on the complex urban structure of Washington DC). To handle this we take advantage of our multivariate setup. Define $X^{\text{pooled}} = \cup_{i=1}^p X_i$ with intensity function $\rho^{\text{pooled}}(\mathbf{u}) = \sum_{i=1}^p \rho_i(\mathbf{u})$. An estimator of ρ^{pooled} is simply given by $\hat{\rho}^{\text{pooled}}(\mathbf{u}) = \hat{\rho}_0(\mathbf{u}) \sum_{i=1}^p \exp(\hat{\beta}_i^\top \mathbf{z}(\mathbf{u}))$. We can then define two different estimators, $\hat{\omega}$ and \hat{w} , for the area of the observation window:

$$\hat{\omega}(b) = \frac{1}{p} \sum_{i=1}^p \sum_{\mathbf{u} \in X_i} \frac{1}{\hat{\rho}_0(\mathbf{u}) \exp(\hat{\beta}_i^\top \mathbf{z}(\mathbf{u}))} \quad \text{and} \quad \hat{w}(b) = \sum_{\mathbf{u} \in X^{\text{pooled}}} \frac{1}{\hat{\rho}^{\text{pooled}}(\mathbf{u})}$$

where the dependence on b is through $\hat{\rho}_0(\cdot)$. We then select the bandwidth b that minimizes $(\hat{\omega}(b) - \hat{w}(b))^2$. Hence, the bandwidth can be selected without specifying the observation window.

F Modification of Diggle et al. (2007)s second order analysis

As pointed out in Diggle et al. (2007), non-parametric estimation of both first and second order properties from the same point pattern data is an ill-posed problem due to confounding between variations in the intensity function and random clustering. In case of a bivariate case-control point process and assuming the model (3), Diggle et al. (2007) suggested to estimate ρ_0 using the control points and plug in this estimate when inferring the clustering properties of the case process. This approach can be extended to the multivariate ($p > 2$) setting as follows. For each type $i =$

$1, \dots, p$ we modify (17) to obtain the estimator

$$\hat{\rho}_{0,-i}(\mathbf{u}) = \frac{1}{p-1} \sum_{\substack{k=1 \\ k \neq i}}^p \sum_{\mathbf{v} \in X_k} \frac{k((\mathbf{u} - \mathbf{v})/b)}{\exp(-\hat{\boldsymbol{\beta}}_k^\top \mathbf{z}(\mathbf{v})) b^d c_b(\mathbf{v})},$$

that does not utilize the i th point pattern. To ease the computation time we estimate one common bandwidth b for all $i = 1, \dots, p$ by the bandwidth selection criterion described in Section E. To estimate the PCFs and cross PCFs we use the `spatstat` procedures `pcfinhom` and `crosspcfinhom`, where we specify the intensity functions by $\hat{\rho}_i(\mathbf{u}) = \hat{\rho}_{0,-i}(\mathbf{u}) \exp(\hat{\boldsymbol{\beta}}_i^\top \mathbf{z}(\mathbf{u}))$. We manually choose the bandwidth for the PCFs and cross PCFs.

G Analysis for tumor cells

For the tumor cells we use 80% independent thinning of the points but otherwise proceed precisely as in Section 5.1.1 to which we refer for details. We choose Normoxic as the baseline and estimate $\boldsymbol{\beta} = (\beta_{\text{Hyp}}, \beta_{\text{Nor}})^\top$ by $\hat{\beta}_{\text{Hyp}} = \log(2346/3693) = -0.45$ and $\hat{\beta}_{\text{Nor}} = 0$. The left panel in Figure 14 shows that the cross validation score is

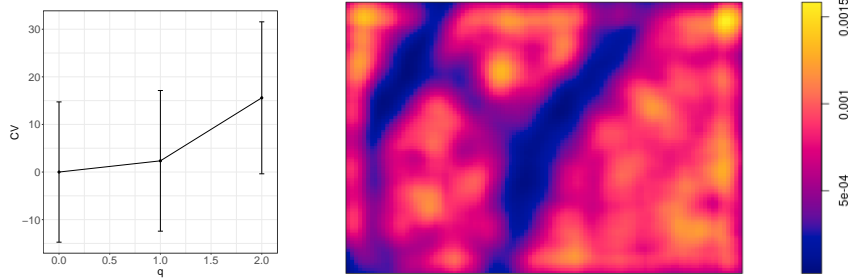


Figure 14: Left: CV-scores (minus minimum CV-score) with standard errors. Right: Non-parametric estimate of ρ_0 with bandwidth = 153.3.

minimized for $q = 0$. Hence, we model the bivariate point process as two independent LGCPs. The right panel in Figure 14 shows the non-parametric estimate of ρ_0 .

The parameter estimates with $q = 0$ are $\hat{\sigma}_{\text{Hyp}} = 1.45$, $\hat{\sigma}_{\text{Nor}} = 1.31$, $\hat{\phi}_{\text{Hyp}} = 66.1$, and $\hat{\phi}_{\text{Nor}} = 46.4$. The estimates of σ_{Hyp} and σ_{Nor} show that in addition to the variation caused by ρ_0 , both the Hypoxic and Normoxic cells are highly clustered with strongest clustering for Hypoxic. This is also illustrated by the fitted PCFs in the left panel of Figure 15.

Figure 15 shows that the agreement between the semi-parametric and consistent non-parametric estimates of cross PCF ratios $g_{\text{Hyp}}/g_{\text{Nor}}$ and $g_{\text{Hyp,Nor}}/g_{\text{Nor}}$ is very good which is confirmed by global envelope p -values of 0.98 in case of $g_{\text{Hyp}}/g_{\text{Nor}}$ and 0.178 for $g_{\text{Hyp,Nor}}/g_{\text{Nor}}$, see also the global envelope plots in Section H. The conclusions regarding the simple non-parametric estimates shown in Figure 15 (left) are completely analogous to those for Stroma and CD8: the non-parametric estimates seem biased and the simple non-parametric estimates of cross PCF ratios deviate

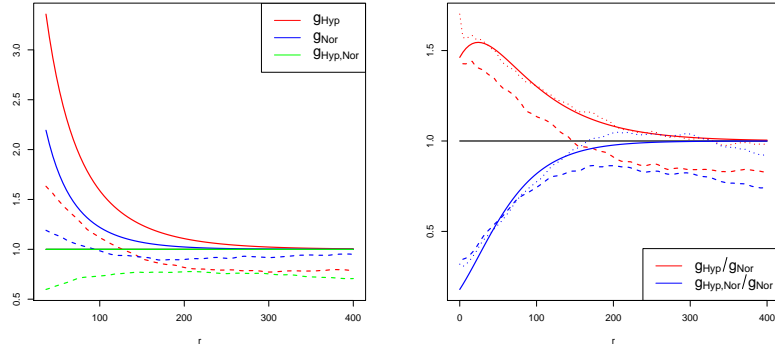


Figure 15: Left: estimated (cross) PCFs using the semi-parametric model (solid) and simple approach (dashed). Right: estimated (cross) PCF ratio using semi-parametric model (solid), simple approach (dashed) and consistent approach (dotted).

more from the consistent non-parametric estimates than the semi-parametric estimates.

H Model assessment for lymphoma data

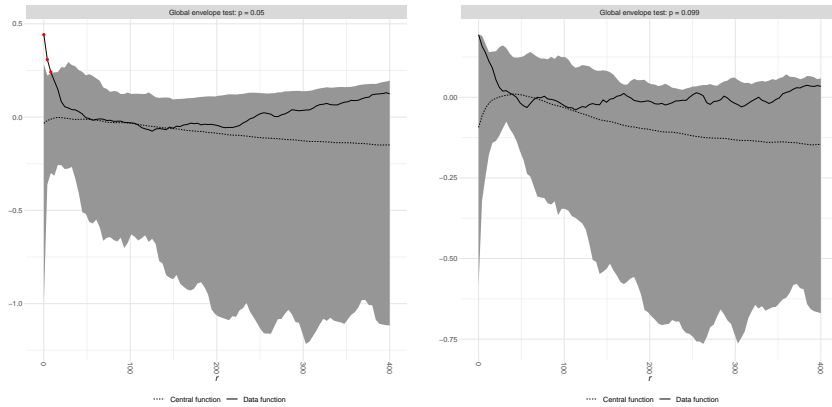


Figure 16: Differences between semi-parametric and consistent non-parametric estimates of cross PCF ratios (solid curves) with global 95% envelopes (gray shaded areas). Left: g_{Str}/g_{CD8} . Right: $g_{Str,CD8}/g_{CD8}$.

I Model assessment for crime data

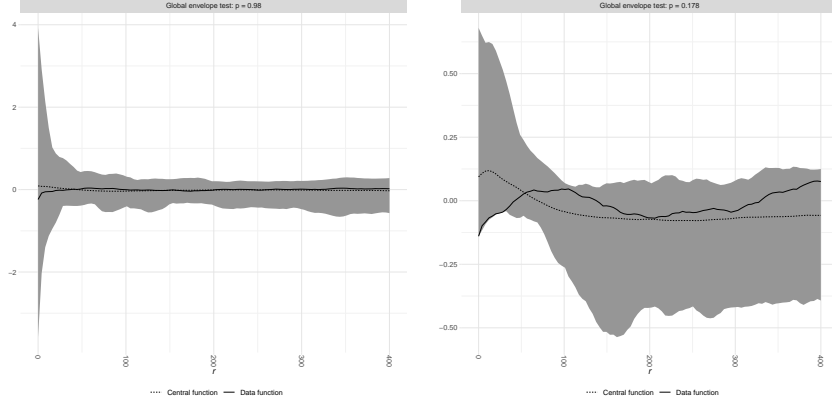


Figure 17: Differences between semi-parametric and consistent non-parametric estimates of cross PCF ratios (solid curves) with global 95% envelopes (gray shaded areas). Left: $g_{\text{Hyp}}/g_{\text{Nor}}$. Right: $g_{\text{Nor,Hyp}}/g_{\text{Nor}}$.

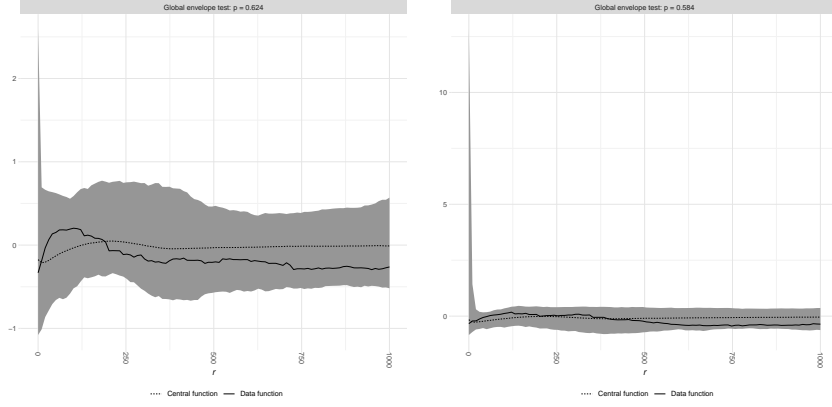


Figure 18: Differences between semi-parametric and consistent non-parametric estimates of cross PCF ratios (solid curves) with global 95% envelopes (gray shaded areas). Left: g_1/g_6 . Right: g_2/g_6 .

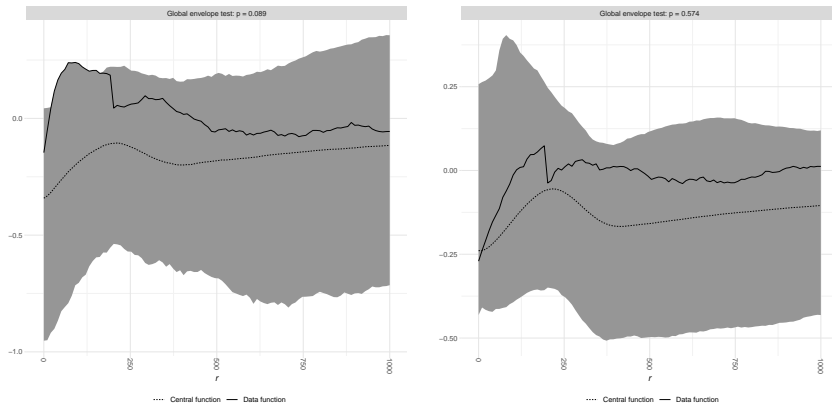


Figure 19: Differences between semi-parametric and consistent non-parametric estimates of cross PCF ratios (solid curves) with global 95% envelopes (gray shaded areas). Left: g_{13}/g_6 . Right: g_{16}/g_6 .

References

- Baddeley, A., A. Jammalamadaka, and G. Nair (2014). Multitype point process analysis of spines on the dendrite network of a neuron. *Journal of the Royal Statistical Society: Series C* 63, 673–694.
- Baddeley, A., E. Rubak, and R. Turner (2015). *Spatial Point Patterns: Methodology and Applications with R*. CRC Press.
- Baddeley, A. J., J. Møller, and R. Waagepetersen (2000). Non- and semi-parametric estimation of interaction in inhomogeneous point patterns. *Statistica Neerlandica* 54, 329–350.
- Choiruddin, A., F. Cuevas-Pacheco, J.-F. Coeurjolly, and R. Waagepetersen (2019). Regularized estimation for highly multivariate log Gaussian Cox processes. *Statistics and Computing* 30, 649–662.
- Cronie, O. and M. N. M. van Lieshout (2016). Summary statistics for inhomogeneous marked point processes. *Annals of the Institute of Statistical Mathematics* 68, 905–928.
- Cronie, O. and M. N. M. van Lieshout (2018). A non-model-based approach to bandwidth selection for kernel estimators of spatial intensity functions. *Biometrika* 105, 455–462.
- Diggle, P. J., V. Gómez-Rubio, P. E. Brown, A. G. Chetwynd, and S. Gooding (2007). Second-order analysis of inhomogeneous spatial point processes using case-control data. *Biometrics* 63, 550–557.
- Guan, Y., R. Waagepetersen, and C. M. Beale (2008). Second-order analysis of inhomogeneous spatial point processes with proportional intensity functions. *Journal of the American Statistical Association* 103, 769–777.
- Hastie, T., R. Tibshirani, and J. Friedman (2013). *The Elements of Statistical Learning* (2 ed.). Springer Series in Statistics. New York, NY, USA: Springer New York Inc.
- Henrys, P. and P. Brown (2009, June). Inference for clustered inhomogeneous spatial point processes. *Biometrics* 65, 423–430.
- Hessellund, K. B., G. Xu, Y. Guan, and R. Waagepetersen (2019). Semi-parametric multinomial regression for multivariate point pattern data. Under revision.
- Jalilian, A., Y. Guan, J. Mateu, and R. Waagepetersen (2015). Multivariate product-shot-noise Cox models. *Biometrics* 71, 1022–1033.
- Lavancier, F., A. Poinas, and R. Waagepetersen (2019). Adaptive estimating function inference for nonstationary determinantal point processes. *Scandinavian Journal of Statistics*. Appeared online.

- Møller, J. and R. Waagepetersen (2003). *Statistical inference and simulation for spatial point processes*. Boca Raton: Chapman and Hall/CRC.
- Myllymäki, M., T. Mrkvička, P. Grabarnik, H. Seijo, and U. Hahn (2016). Global envelope tests for spatial processes. *Journal of the Royal Statistical Society, Series B* 79, 381–404.
- Rajala, T., D. J. Murrell, and S. C. Olhede (2018). Detecting multivariate interactions in spatial point patterns with Gibbs models and variable selection. *Journal of the Royal Statistical Society, Series C* 67, 1237–1273.
- Shaw, T., J. Møller, and R. Waagepetersen (2020). Globally intensity-reweighted estimators for K - and pair correlation functions. *Australian and New Zealand Journal of Statistics*. Accepted for publication.
- Shi, P., A. Zhang, and H. Li (2016). Regression analysis for microbiome compositional data. *Annals of Applied Statistics* 10, 1019–1040.
- Tibshirani, R. (1996). Regression shrinkage and selection via the Lasso. *Journal of the Royal Statistical Society, Series B* 58, 267–288.
- van Lieshout, M. N. M. (2011). A J -function for inhomogeneous point processes. *Statistica Neerlandica* 65, 183–201.
- Waagepetersen, R. and Y. Guan (2009). Two-step estimation for inhomogeneous spatial point processes. *Journal of the Royal Statistical Society, Series B* 71, 685–702.
- Waagepetersen, R. P., Y. Guan, A. Jalilian, and J. Mateu (2016). Analysis of multispecies point patterns by using multivariate log-Gaussian Cox processes. *Journal of the Royal Statistical Society, Series C* 65, 77–96.